ACS Energy LETTERS

http://pubs.acs.org/journal/aelccp

PERSPECTIVE

Semiconducting Single-Walled Carbon Nanotubes in Solar Energy Harvesting

Jeffrey L. Blackburn*

National Renewable Energy Laboratory, Golden, Colorado 80401, United States

ABSTRACT: Semiconducting single-walled carbon nanotubes (s-SWCNTs) represent a tunable model one-dimensional system with exceptional optical and electronic properties. High-throughput separation and purification strategies have enabled the integration of s-SWCNTs into a number of optoelectronic applications, including photovoltaics (PVs). In this Perspective, we discuss the fundamental underpinnings of two model PV interfaces involving s-SWCNTs. We first discuss s-SWCNT−fullerene heterojunctions where exciton dissociation at the donor−acceptor interface drives solar energy conversion. Next, we discuss charge extraction at the interface between s-SWCNTs and a photoexcited perovskite active layer. In each case, the use of highly enriched semiconducting SWCNT samples enables fundamental insights into the thermodynamic and kinetic mechanisms that drive the efficient conversion of solar photons into long-lived separated charges. These model systems help to establish design rules for next-generation PV devices containing well-defined organic semiconductor layers *and* help to frame a number of important outstanding questions that can guide future studies.

Since their discovery in the early 1990s,[1,2] single-walled carbon nanotubes (SWCNTs) have been studied intensively for their unique optical, electrical, and physical properties, as well as for myriad devices and applications. SWCNTs can have either semiconducting or metallic electronic structure depending on their diameter and chiral angle, geometric properties that are captured by the unique "(n,m) chiral indices" assigned to each particular SWCNT species. Many applications depend critically on particular optical and/or electrical properties, such as charge carrier density and type, band gap, and frontier orbital energy levels. As such, the ability to effectively separate semiconducting (s)- and metallic (m)-SWCNTs was a crucial turning point in the evolution of SWCNT research in the mid- to late 2000s.[3−6] In the past 10 years, a number of different high-throughput separation techniques have been developed,[7,8] and the past 5 years have witnessed a strong resurgence of both fundamental and applied SWCNT research, based on the ultrapure SWCNTs that are now available.

S-SWCNTs are advantageous for a number of important applications. They emit light in regions of the electromagnetic spectrum in which blood and tissue have little absorption and autofluorescence, making them attractive for biological imaging.[9−11] Narrow emission line widths, tunable within the region of the spectrum utilized for telecommunications, make them attractive as elements in telecommunications systems (e.g., optical switches, signal converters, or signal regenerators).[12−14] Isolated sp^3 defects have also been shown to enable highly efficient single-photon emission, encouraging their use as single-photon sources for, for example, telecommunications or quantum computing.[15] The tunable (and moderately large) s-SWCNT band gap, along with very high carrier mobility, have enabled their demonstration in both high-performance narrow-channel field effect transistors (FETs) and thin-film FETs.[16−18] S-SWCNTs are also useful in thermoelectric (TE) energy harvesting applications, in part due to the fact that the one-dimensional density of states (DOS) imparts s-SWCNTs with very large Seebeck coefficients (thermopower).[19,20] When these high thermopowers are paired with the ability to tune the carrier density via doping and extremely high charge carrier mobilities and conductivities, s-SWCNT thin films produce large TE power factors that are on par with the best semiconducting polymers.

> Semiconducting SWCNTs occupy a unique space in the world of semiconductors, with properties that span those of organic molecules, semiconducting polymers, and solid-state semiconductors.

When analyzing their utility in solar energy harvesting, it is important to consider that s-SWCNTs occupy a unique space in

Received: March 14, 2017
Accepted: May 31, 2017

DOI: 10.1021/acsenergylett.7b00228
ACS Energy Lett. 2017, 2, 1598−1613

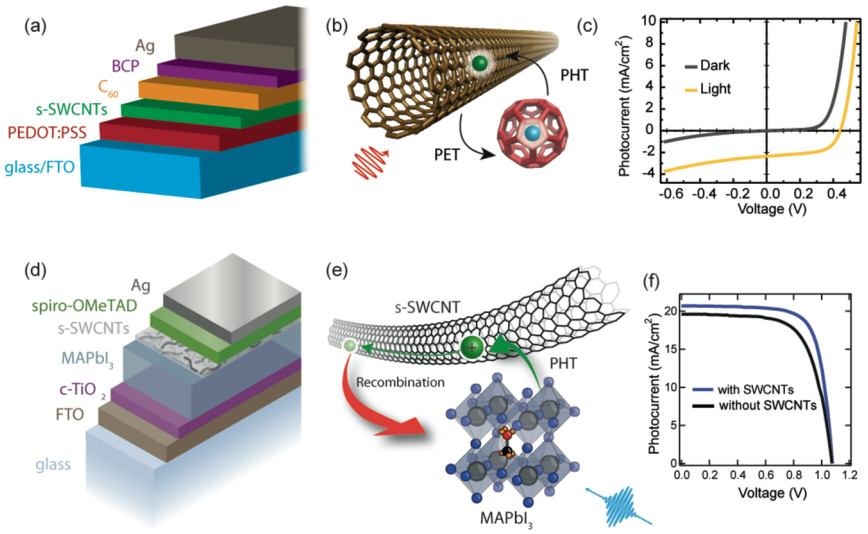

Figure 1. SWCNT energy harvesting systems covered in this Perspective. (a) Schematic of the SWCNT−C_{60} solar cell. (b) Charges are generated in these devices by photoinduced electron transfer (PET) or photoinduced hole transfer (PHT) at the SWCNT−C_{60} interface. (c) J−V curve of a representative SWCNT−C_{60} solar cell. (d) Schematic of a $MaPbI_3$ solar cell, using a s-SWCNT interfacial layer to extract holes. (e) Fast PHT is observed from $MAPbI_3$ to s-SWCNTs, while recombination is slow. (f) J−V curve of a representative $MAPbI_3$ solar cell with and without a s-SWCNT hole extraction layer, only showing the fourth quadrant. Panels (a−c) are adapted from ref 60 with permission from the Royal Society of Chemistry, and panels (d−f) are adapted from ref 93 with permission from the Royal Society of Chemistry.

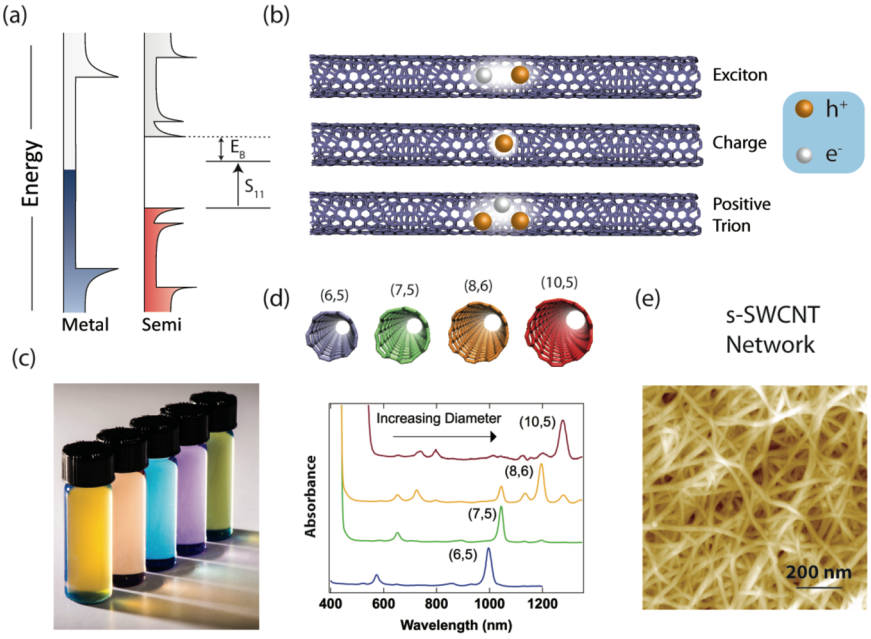

Figure 2. Basic properties and separations of s-SWCNTs. (a) (Left) Single-particle DOS for m- and s-SWCNTs. (Right) Optical transitions, such as the depicted S_{11}, are excitonic, with a characteristic binding energy (E_b). (b) Three different excited states of s-SWCNTs. (c,d) Photos (photo credit to Dennis Schroeder, https://images.nrel.gov) and absorption spectra of highly enriched s-SWCNT inks prepared by polyfluorene extraction. (e) AFM image of a s-SWCNT film prepared by ultrasonic spraying of an ink similar to those shown in panel (c). Panel (e) is reprinted with permission from ref 20 Copyright 2016 American Chemical Society.

the world of semiconductors, with properties that span those of organic molecules, semiconducting polymers, and solid-state semiconductors. In many ways, their delocalized π electron system imparts properties that evoke those of small conjugated molecules, oligomers, or semiconducting polymers. In other ways, their well-defined extended periodic lattice and relatively small carrier mass invoke comparisons to inorganic solid-state semiconductors. S-SWCNTs have molecule-like absorption, with extremely narrow excitonic and vibronic resonances, and also have defined chirality, in which mirror-image enantiomers exhibit strong circular dichroism.[21] However, unlike their molecular analogues, s-SWCNTs have gigantic aspect ratios with a regular periodic lattice that may extend for thousands of unit cells, a property much more in line with inorganic semiconducting nanowires. Absorption of photons by s-SWCNTs creates bound electron−hole pairs, or excitons, with a characteristic binding energy (E_b) and correlation length (ξ_e).[22,23] S-SWCNT excitons are tightly bound, which is typical for the Frenkel-type excitons characteristic of molecular solids, but the size of the exciton is much larger than the lattice constant,

DOI: 10.1021/acsenergylett.7b00228
ACS Energy Lett. 2017, 2, 1598−1613

more in line with the Wannier excitons' characteristic of covalent inorganic semiconductors. As with semiconducting polymers, charge transport in s-SWCNTs is facilitated by the extended π electron network. However, s-SWCNTs are quite rigid and have small effective carrier mass,[24] high charge carrier mobility,[25] and low internal reorganization energy,[26] in strong contrast to typical semiconducting polymers that are dominated by polaron transport.[27]

The intriguing properties discussed above make a compelling case for the study of s-SWCNTs as active elements in a number of energy-related technologies, such as batteries, fuel cells, photovoltaics (PVs), solar fuels, and TEs. In this Perspective, we will focus specifically on concepts and studies related to solar energy harvesting, in which electromagnetic radiation in the visible and infrared regions of the spectrum are converted into electricity. In particular, we will examine the fundamental mechanisms governing the function of s-SWCNTs in two model PV energy harvesting schemes, one where the s-SWCNTs serve as a primary absorptive component of the active layer and another where the s-SWCNTs serve as passive charge extraction layers for perovskite solar cells (Figure 1).

Basic Properties of Semiconducting SWCNTs. Numerous reviews have covered the fundamental electronic structure of single-walled carbon nanotubes; therefore, we refer the interested reader to these reviews for a more detailed treatment.[28] Most important for the current discussion is the fact that SWCNTs can have either semiconducting or metallic electronic structure, depending on the particular diameter and chiral angle of the SWCNT in question. Statistically, in most SWCNT syntheses, 1/3 of the SWCNTs are metallic and 2/3 are semiconducting. Figure 2a displays calculated DOSs for representative s- and m-SWCNTs. Each type of SWCNT has sharp peaks in the DOS called van Hove singularities (VHS) that arise from two-dimensional quantum confinement. In m-SWCNTs, there is a finite DOS in between the lowest conduction and valence VHS, and the lowest-energy ground-state electrons reside at the Fermi energy in the middle of the gap. In contrast, s-SWCNTs have no DOS in between the lowest-energy conduction and valence VHS, and the lowest-energy electrons (in undoped s-SWCNTs) reside at the top of the valence VHS.

Commonly synthesized s-SWCNTs (e.g., with diameters between ~0.7 and 2.0 nm) have electronic band gaps (the energy difference between the lowest-energy conduction and electron VHS) in the range of 0.5−1.7 eV. Strong Coulomb interactions give rise to significant electron−hole binding energies such that photoexcited electron−hole pairs in s-SWCNTs are stabilized as bound excitons, with exciton binding energies in the range of 0.2−0.5 eV (Figure 2a,b).[23] The optically active excitonic transitions are narrow, with resolution-limited line widths on the order of ~40 μeV having been recently measured for isolated s-SWCNTs at 4 K.[29] Inhomogeneous broadening leads to room-temperature excitonic line widths on the order of 40 meV (for a single (n,m) species) for the ensemble samples that are typically utilized in macroscopic applications.[30] S-SWCNT excitonic transitions have strong absorption coefficients, in the range of 4400 $M^{-1}cm^{-1}$, with oscillator strengths in the range of 0.010 per carbon atom (cross section of $1-2 \times 10^{-17}$ cm^2/C).[31] The oscillator strengths for excitonic transitions are related to the spin, symmetry, and momentum selection rules associated with both the single-particle DOSs from which a particular transition is derived and many-body interactions.[32] The dominant bright transitions are Γ-momentum singlet excitons arising from VHS of equivalent quantum number (n) where $\Delta n = 0$ (e.g., S_{11}, S_{22}, S_{33}) and with transition dipole parallel to the s-SWCNT axis. A variety of weakly allowed and/or dark transitions are also present for s-SWCNTs, including dipole-forbidden excitonic transitions,[33,34] weakly allowed cross-polarized transitions (e.g., S_{12}, S_{21}, S_{24}, etc.),[21,35] vibronic transitions (e.g., K-momentum, herein denoted X_{11}, etc.),[30,36,37] and spin-forbidden transitions (e.g., triplets, T_1, T_2, etc.).[38] Finally, many-body quasi-particles, such as biexcitons[39] and trions (a three-body particle consisting of an exciton bound to a charge),[40,41] are also commonly observed in photoexcited s-SWCNTs due to the strong Coulomb interaction (Figure 2b). The utilization of s-SWCNTs in PV applications depends crucially on this rich spectrum of optical transitions for this unique semiconductor.

Separations of SWCNTs to Achieve Highly Pure s-SWCNTs. Tremendous progress has been made in the separation of SWCNTs into type-pure samples over the past decade. Many techniques are now available, each technique having potential advantages and disadvantages in terms of yield, throughput, and requirements for postseparation workup. The four predominant routinely utilized separation techniques are density gradient ultracentrifugation (DGU),[3,42] gel column chromatography (GCC),[5,43] aqueous two-phase extraction (ATPE),[44−46] and selective polymer extraction (SPE).[4,8] The first three are all aqueous separation techniques, while SPE is typically performed in organic solvents such as toluene.

All of the aqueous techniques rely on the diameter- and electronic structure-specific packing structure of surfactant mixtures on SWCNT surfaces. DGU is based on the influence of this packing structure on the SWCNT buoyant density. In GCC, the separation mechanism relies on the influence of these packing structures on the adsorption affinity for a stationary gel such as agorose or dextran.[43,47] ATPE relies on the influence of these packing structures on the SWCNT hydrophobicity and the resulting affinity for one of two phases with varying hydrophobicity (typically poly(ethylene glycol) and dextran). The most commonly employed surfactants in these separations are sodium dodecyl sulfate (SDS), sodium cholate (SC), and sodium deoxycholate (DOC), and DNA-based variations on these techniques have also been very effective at producing samples highly enriched in particular (n,m) species. All of the techniques have demonstrated successful separations based on electronic structure (semiconducting versus metallic), diameter, chiral angle (specific (n,m) species), and even optical isomers of specific species (left- versus right-handed enantiomers).[21,42,48]

SPE is a relatively rapid method for producing highly enriched s-SWCNTs.[4,8] This method relies on the large difference in noncovalent binding affinity for polyfluorene (and some other) polymers on either s- or m-SWCNTs.[49] Thus, simply sonicating a polydisperse batch of as-synthesized SWCNTs with an appropriate concentration of a wide variety of polyfluorene polymers, followed by light centrifugation, produces dispersions that are highly enriched in s-SWCNTs. The method has now been used to produce highly enriched s-SWCNT dispersions using starting materials from any synthetic method and diameter distribution. Certain polyfluorene polymers disperse all s-SWCNTs within a raw soot without selecting specific species, while others are highly selective for certain (n,m) species or families of s-SWCNTs (e.g., near-armchair).[4,8] Recent advances to this technique include the development of "degradable" polymers that incorporate specific bonds between monomer units that can be attacked following extraction.[50−54] The methods of postextraction degradation include breaking imine

DOI: 10.1021/acsenergylett.7b00228
ACS Energy Lett. 2017, 2, 1598−1613

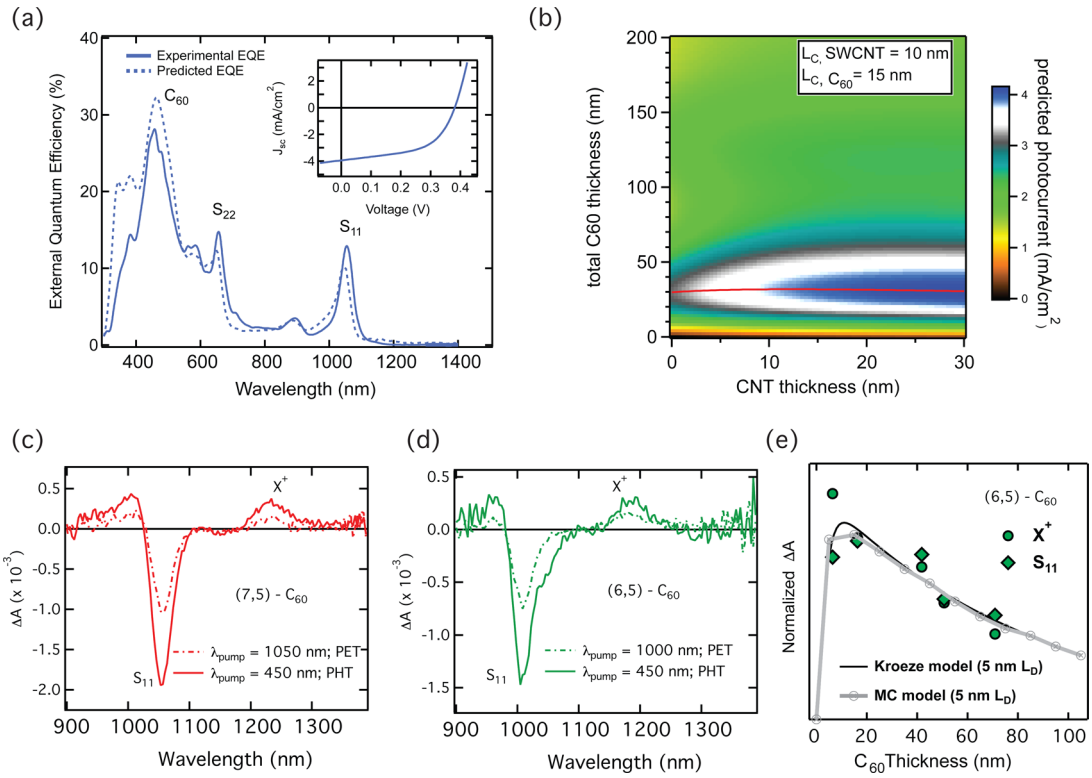

Figure 3. Estimating exciton diffusion lengths in SWCNT−C_{60} bilayers. (a) Comparison of the experimental EQE to the EQE predicted by using the model in panel (b) for a solar cell with a 10 nm (7,5) SWCNT layer and a 32 nm C_{60} layer. (Inset) J−V curve for the device. (b) 2D map of predicted J_{SC} for devices with varying (7,5) SWCNT and C_{60} layer thickness. (adapted from ref 60 with permission from the Royal Society of Chemistry). This prediction assumes a capture length (L_C, the length scale over which excitons are effectively transported to the interface to be dissociated) of 10 nm for the SWCNT layer and 15 nm for the C_{60} layer. L_C does not include reflection of excitons at surfaces opposite the heterojunction interface and is thus an upper limit for the exciton diffusion length, L_D. (c,d) Transient absorption spectra of charged (c) (7,5) s-SWCNTs and (d) (6,5) s-SWCNTs following PET or PHT at the SWCNT−C_{60} interface. (e) The SWCNT bleach (S_{11}) and trion induced absorbance (X^+) can be used as reporters to track exciton diffusion to the SWCNT−C_{60} interface. In panel (e), two different models are used to estimate a diffusion length, L_D, of ∼5 nm in the C_{60} layer for a (6,5)−C_{60} bilayer. Panel (e) is reprinted with permission from ref 41 Copyright 2016 American Chemical Society.

or hydrogen bonds with acids, photodegradation, and decomplexation of dative transition metal coordination bonds.

For a number of reasons, our own recent work on energy harvesting with s-SWCNTs has focused almost exclusively on samples generated by selective extraction with polyfluorenes (Figure 2c−e). This technique has been shown to generate extremely high purities of s-SWCNTs, with metal impurities as low as 0.001% suggested by recent FET studies.[16] The technique also has very high yield and throughput,[8] generating high-concentration inks rapidly (Figure 2c), an important quality for scalable deposition and fabrication of energy harvesting devices. The technique enables the extraction of a wide variety of s-SWCNT band gaps (Figure 2d), making it quite versatile for generating inks and thin films that can harvest energy in various regions of the spectrum. Finally, the inks generated by selective extraction are easily integrated into scalable deposition techniques, such as ultrasonic spraying, that enable the rapid deposition of uniform thin films with controllable thickness (Figure 2e). Because the inks utilize organic solvents, they can be deposited directly onto surfaces that degrade in contact with water, such as perovskites.

S-SWCNTs as Active Elements in Solar Energy Harvesting. SWCNT solar cells represent one variation of a broad class of PVs that can be termed excitonic solar cells.[55] In excitonic solar cells, the primary quasi-particle created by absorption of a photon is an exciton, where the electron and hole are Coulombically bound with an exciton binding energy well in excess of the thermal energy (kT). To generate the separated charge carriers needed to produce photocurrent, excitonic solar cells typically feature a donor−acceptor interface where a thermodynamic driving force of appropriate magnitude supplies the requisite energy to dissociate excitons via interfacial charge transfer. The thermodynamic driving force (ΔG) is related to the frontier orbital energies of the donor and acceptor species, as well as the exciton energy of the component being photoexcited through the equation

$$\Delta G = |\mathrm{IP_D} - \mathrm{EA_A}| - E_{ex} \quad (1)$$

In eq 1, $\mathrm{IP_D}$ is the ionization potential of the donor, $\mathrm{EA_A}$ is the electron affinity of the acceptor, and E_{ex} is the energy of the exciton (optical band gap of the component being photoexcited). The exciton energy in turn incorporates the binding energy

$$E_{ex} = E_{el} - E_b \quad (2)$$

In eq 2, E_{el} is the electronic band gap (energy difference between the IP and EA of the component being photoexcited) and E_b is the exciton binding energy.

To understand how an excitonic solar cell functions and to optimize the efficiency of such a PV, it is important to consider a series of fundamental steps that occur over a variety of time scales. The most important events include (1) absorption of a photon to create an exciton, (2) diffusion of the exciton to the

DOI: 10.1021/acsenergylett.7b00228
ACS Energy Lett. 2017, 2, 1598−1613

donor−acceptor interface, (3) dissociation of the exciton via interfacial electron or hole transfer, and (4) migration and/or diffusion of each charge carrier to the appropriate electrode where it is collected. This series of desired steps is in constant competition with a number of undesired pathways that can lead to loss of the energy associated with photon absorption, including (1) exciton recombination, (2) exciton−exciton annihilation or other collisional Auger processes, and (3) charge trapping and/or recombination. This competition between the events that lead to the successful collection of energetic charge carriers and the deleterious events that deactivate excitons and charges all comes down to the relative rates of the numerous events that excitons and charges undergo.

Here, we discuss what has been learned about the mechanisms and rates of these various processes for SWCNT donor−acceptor PV blends. Two general types of SWCNT organic PV blends have been studied extensively, polymer−SWCNT blends where the SWCNTs act as electron acceptors[56,57] and SWCNT−fullerene bilayers and blends where the SWCNTs act as electron donors.[26,40,41,58−69] We focus here on the latter class of materials because the studies of these types of interfaces have focused heavily on the direct contribution of photoexcited SWCNTs to the design and function of the solar cell. SWCNT−fullerene bilayer solar cells were first demonstrated by the Arnold group in 2011.[65] In these solar cells, photoexcited excitons created in either the SWCNT layer or fullerene layer can be dissociated at the SWCNT−fullerene interface by either electron or hole transfer, respectively. Figure 3a shows a $J-V$ curve and external quantum efficiency (EQE) spectra for a representative s-SWCNT−C_{60} thin-film solar cell. Contributions to the photocurrent from both the (7,5) s-SWCNT (electron transfer to C_{60}) and the C_{60} (hole transfer to (7,5)) can be seen in the EQE. Because these devices are quite thin and contain a reflective silver electrode on the back of the cell, the optical field within the device depends sensitively on the exact thickness of each layer.[60] Thus, the relative contributions of either the s-SWCNT or fullerene layer can be tuned and can also be modeled by using the thickness and optical constants of each layer to calculate the position-dependent optical field within the device (Figure 3b and predicted EQE in Figure 3a).[60]

Exciton Diffusion. The first important requirement for these bilayer heterojunctions, following photon absorption, is the successful transport of excitons within either layer to the SWCNT−fullerene interface. Arnold, Zanni, and co-workers have performed a number of studies on exciton diffusion within thin s-SWCNT films, utilizing both photocurrent studies on bilayer devices and ultrafast optical studies on bare s-SWCNT films.[70−73] Early device studies demonstrated that the diffusion length of s-SWCNT excitons (L_d) to the SWCNT−fullerene interface was quite short, in the range of 5−10 nm. This value of L_d is far below what has been measured for the intratube L_d (several hundreds of nm) and points to tube−tube junctions as a limiting factor for exciton transport in s-SWCNT networks. L_d appears to be limited, at least in part, by the residual polyfluorene polymer that remained within these thin s-SWCNT films and presumably acts as a barrier to efficient intertube exciton hopping.

Recent studies from the Wisconsin group have utilized polarization-sensitive one-dimensional and two-dimensional ultrafast transient absorption (TA) to follow exciton transport within thin films containing either multiple s-SWCNT species or one primary s-SWCNT species (e.g., (7,5)).[70−73] These studies suggest multiple mechanisms for exciton transport, depending on the s-SWCNT distribution and amount of residual polyfluorene wrapping polymer within the film. For multispecies films containing residual polymer, some excitons transferred rapidly from the initially excited s-SWCNTs to other s-SWCNTs with equivalent or smaller band gaps, with time scales in the subpicosecond range. Another subpopulation of excitons was found to diffuse to the tube−tube crossing points and hop from tube to tube on a slower time scale of several picoseconds. In studies comparing films with and without polyfluorene, the time scale for diffusion-assisted hopping between SWCNTs is dramatically faster (subpicosecond) without the wrapping polymer.[72,73] This is an encouraging result and will likely lead to bilayer devices with improved L_d. Our own studies suggest that the identity of the polymer, in particular, the degree to which particular polymers leave open space on the SWCNT surface, may play an important role in determining the degree of exciton diffusion within the bulk of the s-SWCNT film.[74]

Excitons generated within the fullerene phase must also diffuse to the interface, where interfacial hole transfer drives charge separation. This exciton diffusion process can be followed in real time using TA spectroscopy.[41] In this experiment, spectral signatures of charges in the s-SWCNTs are used as reporters to track the time required for excitons to diffuse through the fullerene layer to the interface and dissociate. In TA experiments, two distinct s-SWCNT signals can be used as signatures of charges in the s-SWCNTs (Figure 3c,d): (1) a photoinduced first exciton (S_{11}) bleach and (2) a photoinduced absorption caused by the absorbance of a trion quasi-particle (X^+).[40,41] A trion is a three-body quasi-particle that consists of an exciton bound to a charge carrier (Figure 2b). Due to the strong Coulomb interaction in s-SWCNTs, trions are quite stable at room temperature, with an absorption energy ∼170 meV below S_{11}.[75,76] Using the S_{11} and X_1 transitions as reporters for charges, we found an exciton diffusion length of ∼5 nm within the fullerene phase.[41] This technique was also developed, essentially simultaneously with our own studies, for tracking exciton diffusion in C_{70} layers by using the photoinduced absorption of hole polarons in a semiconducting polymer as the reporter for interfacial charge transfer.[77]

Exciton Dissociation. Once at the interface, excitons are dissociated to produce the requisite unbound charges. As captured in eqs 1 and 2, the thermodynamic driving force for exciton dissociation arises from the energetic offsets in the frontier orbital energies of the donor and acceptor. However, the rate of this process depends on several critical parameters of the interface in question: (1) the thermodynamic driving force for photoinduced electron transfer (PET) (ΔG_{PET}), (2) the donor−acceptor electronic coupling (A_{PET}), and (3) the reorganization energy (λ). As described originally by Marcus, these parameters define the rate constant of PET (k_{PET}) at a given temperature (T)

$$k_{PET} = A_{PET} \exp\left[\frac{-(\lambda + \Delta G_{PET})^2}{4\lambda k_B T}\right] \quad (3)$$

The reorganization energy quantifies the response of the system to the charge transfer event. The photoinduced charge transfer event takes the donor−acceptor pair from being electrically neutral (uncharged) to a state where the donor is positively charged and the acceptor is negatively charged. Importantly, this change in charge state leads to molecular-level changes in, for example, bond lengths and angles for both the donor and acceptor and any surrounding molecules (solvent, matrix, etc.). The energy required to initiate these changes is captured as the

DOI: 10.1021/acsenergylett.7b00228
ACS Energy Lett. 2017, 2, 1598−1613

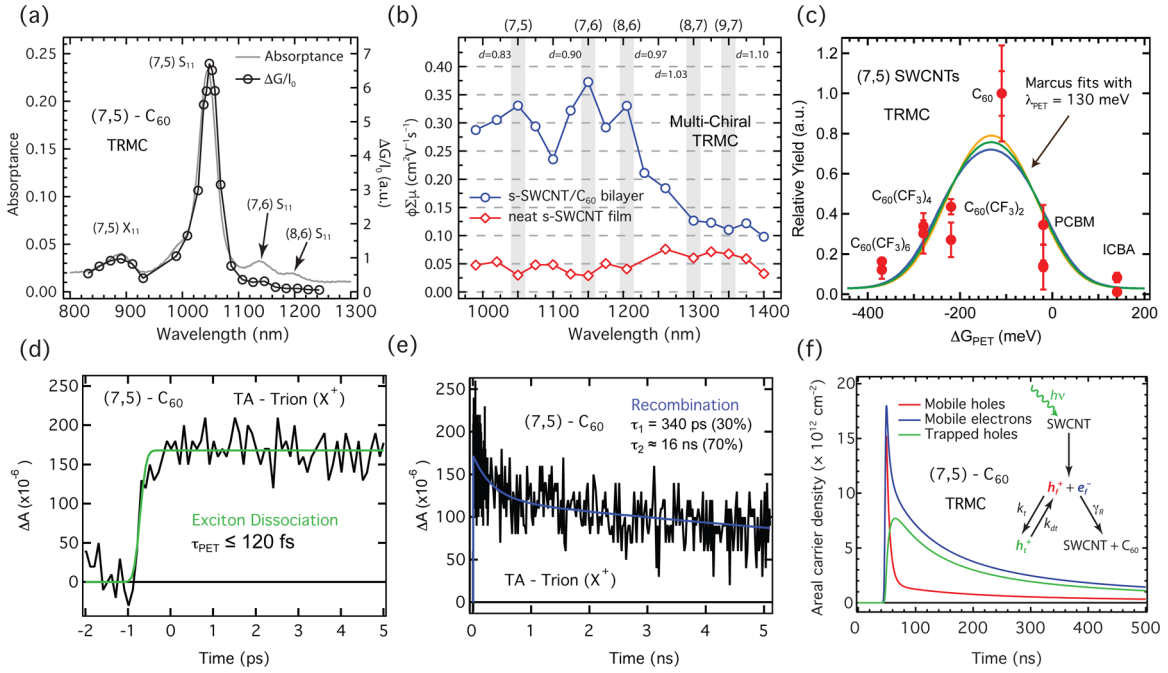

Figure 4. Tracking exciton dissociation and charge recombination in SWCNT−C_{60} bilayers. (a) Photoconductance action spectrum of charge generation in a (7,5)−C_{60} bilayer, measured with TRMC. (b) The magnitude of the photoconductance ($\Phi\sum\mu$) depends crucially upon the s-SWCNT diameter/bandgap in a multichiral s-SWCNT−C_{60} bilayer, suggesting a dependence on the energetic driving force for interfacial PET (ΔG_{PET}). (Reprinted with permission from ref 58 Copyright 2016 American Chemical Society). (c) This dependence on ΔG_{PET} is confirmed by pairing (7,5) s-SWCNTs with fullerene acceptors that have precisely controlled electron affinities. The relative yield of exciton dissociation can be modeled within the Marcus framework to estimate a reorganization energy (λ_{PET}) of ∼130 meV. (Adapted from ref 26 with permission from Nature Publishing Group). The kinetics of (d) interfacial PET and (e) charge recombination can be followed with TA by following the trion induced absorbance. (f) Recombination can also be tracked over longer time scales using TRMC. Global modeling of the TRMC transients are consistent with a recombination process that is limited by capture and emission at traps or states at the SWCNT−C_{60} interface. (Panel (f) adapted from ref 59 with permission from the American Physical Society).

internal reorganization energy (λ_{in} − donor−acceptor) and external reorganization energy (λ_{ex} − surrounding medium).

In a series of recent studies, we set out to unravel the dependence of PET rate and yield on the energetics of model s-SWCNT−fullerene donor−acceptor bilayers (Figure 4).[26,40,58,59] In several studies, we used time-resolved microwave conductivity (TRMC, probe energy of ca. 9 GHz) to follow the yield of charge carriers following photoexcitation of s-SWCNTs in either single-species films (Figure 4a,c) or multispecies films (Figure 4b). Following excitation of a (7,5) s-SWCNT−C_{60} bilayer, the 9 GHz photoconductance "action spectrum" overlays the excitonic absorption features of the (7,5) s-SWCNT (Figure 4a), demonstrating that charges are created by dissociation of (7,5) excitons at the interface.[59] In a bilayer film with multiple s-SWCNT species, the yield of charge carriers depends strongly on the diameter of the s-SWCNT being optically excited (Figure 4b),[58] suggesting that ΔG_{PET} (eqs 1−3) may play a key role in determining the efficiency of PET.

To better understand the dependence of interfacial exciton dissociation on ΔG_{PET}, we took advantage of fullerene acceptors modified with trifluoromethyl (CF_3) electron-withdrawing groups for systematic tuning of the fullerene electron affinity values.[26] The frontier orbital energies of fullerenes are sensitive to the number, position, and type of functional groups appended to the fullerene cage. We measured the yield of photoinduced charges that occurred following photoexcitation of model s-SWCNT donor layers when these layers were paired with fullerenes that systematically modified ΔG_{PET}. Because the yield of photoinduced charges is intimately linked to the relative rates of PET and other competing pathways, eq 3 can be rearranged to capture the dependence of the PET yield on ΔG_{PET} and λ.[26] As shown in Figure 4c for the (7,5) s-SWCNT, the yield of photoinduced charges initially rises with increasing driving force, reaches a peak, and then decreases as the driving force continues to increase. The initial rise represents the "normal region" within the Marcus formulation, whereas the subsequent decline in yield at high driving force represents the "inverted region". Simulating the driving-force-dependent yield in Figure 4c enables extraction of the PET reorganization energy, which was found to be in the range of ∼130 meV. This low reorganization energy is likely dominated by the fullerenes and suggests that delocalized charges make relatively minor perturbations to C−C bonds in s-SWCNTs.

TA has also been used to explicitly measure the interfacial electron transfer kinetics for s-SWCNT−fullerene combinations near the peak of the Marcus curve, that is, with optimized driving force (Figure 4d).[40] As discussed above, the photoinduced S_{11} bleach and photoinduced trion absorption (X^+) can both be used to track the generation of charges on s-SWCNTs. We tracked these spectral signatures following photoexcitation of both (6,5) and (7,5) s-SWCNTs at the lowest-energy S_{11} transitions. In both cases, we observed an instrument response-limited rise time for the X^+ induced absorption, indicating that PET from either (6,5) or (7,5) to C_{60} occurs on the time scale of ≤120 fs.[40] This fast PET time scale is likely related to the fact that, as demonstrated by the driving-force-dependent measurements discussed above, the free energy curves of these donor−acceptor combinations enable barrierless PET.[26]

DOI: 10.1021/acsenergylett.7b00228
ACS Energy Lett. 2017, 2, 1598−1613

Charge Recombination. Once charges are separated across the SWCNT−fullerene interface, the lifetime of the separated charges is an important factor determining the ultimate device performance. We have studied recombination of charges separated across the nanotube−fullerene interface ($SWCNT^+$−C_{60}^-) in detail using both femtosecond TA and TRMC (Figure 4e,f). In TA measurements, the slow disappearance of the trion induced absorbance can be used to track charge recombination to ∼5 ns. For (6,5) and (7,5) s-SWCNTs with C_{60}, a simple biexponential fit to the trion decay dynamics suggested that the dominant recombination occurred with a time constant of ≥16 ns (Figure 4e).[40] The TRMC measurement is sensitive only to mobile charges and enables the resolution of much longer time scales. In this experiment, for a SWCNT−C_{60} bilayer containing five different s-SWCNT species, we observed decay dynamics that again could be fit empirically with biexponential kinetics.[58] In this case, a significant number of mobile charge carriers were lost within the first 100 ns, but a large number of charges also persisted for the entire measurement window, that is, ≥500 ns.

In a follow-up TRMC study, we attempted to better understand the origin of the decay kinetics, simplifying the analysis by looking at a single-species (7,5)−C_{60} bilayer.[59] In this case, we identified a kinetic scheme that described the data well via global kinetic analysis covering up to 4 orders of magnitude in volumetric carrier density. The analysis suggested that capture and emission of charge carriers at traps or states at the SWCNT−C_{60} interface limits the recombination in SWCNT−C_{60} bilayers (Figure 4f). The simulations returned trapping and detrapping rate constants of $k_t \approx 7 \times 10^7$ s^{-1} and $k_{dt} \approx 2 \times 10^7$ s^{-1}, respectively, and a bimolecular recombination coefficient of $\gamma_r \approx 1 \times 10^{-16}$ cm^4 $carrier^{-1}$ s^{-1}.

An important conclusion from the suite of measurements discussed above is the large discrepancy between the rates for interfacial charge transfer and charge recombination in appropriately designed SWCNT−fullerene interfaces. For SWCNT−fullerene pairs with an optimized thermodynamic driving force, charge transfer occurs on the time scale of ∼100 fs, whereas unbound charges survive for many hundreds of nanoseconds or longer before recombining. This long-lived charge separation is a key factor enabling the efficient solar photoconversion for these donor−acceptor PVs in the visible and near-infrared. However, it is important to note that this type of long-lived charge separation can be realized in a number of different systems that utilize s-SWCNTs, not just donor−acceptor heterojunctions where the s-SWCNTs act as active light absorbers. In the next section, we focus on recent studies demonstrating the efficient extraction of long-lived charge carriers by s-SWCNTs in prototypical perovskite solar cells, where the s-SWCNTs are passive (optically) charge extraction layers.

S-SWCNTs as Passive Charge Extraction Layers in High-Efficiency PVs. SWCNTs have been studied for over a decade now as passive charge extraction layer elements in PV devices.[78−84] In these solar cells, the primary function of the SWCNTs is to efficiently collect charges (most often, but not always, holes) from the photoexcited active layer. The SWCNT network can be utilized as an interfacial layer in between the active layer and a metallic electrode, or the SWCNT network can serve as the metallic electrode itself. Furthermore, the SWCNT layer can be utilized as a transparent electrode/layer on the side of the solar cell facing the incoming solar flux or can be used as a "back electrode" where transparency is irrelevant. Finally, the electronic characteristics of the SWCNT−absorber junction can vary from Ohmic to rectifying (e.g., Schottky junction), depending on the intended characteristics of the PV device in question. SWCNT charge extraction layers have now been utilized in a wide variety of solar cells, including OPV,[78,81,85,86] CdTe,[82,87] CIGS,[88] silicon (both p- and n-type),[89−91] and perovskite devices.[83,84,92]

In this section, we focus on the most recent application of SWCNT charge extraction layers in hybrid organic−inorganic perovskite solar cells[83,84,93,94] as this application seems uniquely poised for producing high-efficiency, inexpensive, and stable PV devices.[95] Perovskites are a broad class of compounds with the formula ABX_3, where A and B represent different cations and X typically represents a halide anion.[95] Habisreutinger et al. first demonstrated the use of SWCNT hole extraction layers in perovskite PV devices,[83] where the perovskite absorber layer was the prototypical $MAPbI_3$; in this case, the cations are methylammonium (MA, $CH_3NH_4^+$) and lead (Pb^{2+}) and the anion is iodine (I^-). These initial studies demonstrated that hole transport layers of P3HT-wrapped SWCNTs (containing both s- and m-SWCNTs) enabled perovskite solar cells with >15% power conversion efficiency. Moreover, intercalation of an inert polymer matrix (PMMA or polycarbonate) into the SWCNT hole transport materials (HTMs) dramatically improved the stability of devices with respect to both thermal stress and water ingress.[83] A subsequent study from the same authors demonstrated that composite HTMs prepared from P3HT-wrapped SWCNTs and spiro-OMeTAD enabled extraction of holes without the need for doping of the spiro-OMeTAD layer.[84] Because mobile lithium dopant atoms within spiro-OMeTAD HTMs may contribute to degradation of the perovskite active layer, this strategy affords undoped HTMs that should ameliorate one of the several degradation mechanisms known to affect these solar cells.

While these initial studies demonstrated proof-of-principle for the use of SWCNTs to extract charges from perovskite active layers, there are still numerous questions regarding the principles of operation and fundamental design rules for these novel HTMs. These questions include the following: (1) How do the frontier orbital energies of the SWCNTs and the perovskite active layer control the interfacial band alignment? (2) How does the band alignment control the kinetics of charge transfer and recombination across the SWCNT−perovskite interface? (3) How do the charge extraction and recombination kinetics correlate to device efficiency and stability metrics? To begin answering some of these questions, we recently undertook two studies that focused on the use of highly enriched s-SWCNTs for hole extraction from the $MAPbI_3$ perovskite active layer.[93,94] The studies focused primarily on a model SWCNT system that was enriched with nearly exclusively (6,5) s-SWCNTs (wrapped with a bipyridine-based polyfluorene copolymer). The use of such a highly enriched sample, with primarily one s-SWCNT species, has some clear advantages for making unambiguous conclusions regarding the questions listed above. As opposed to polydisperse samples of SWCNT species, this model system is more like a molecular system, with well-defined redox potentials associated with the electron affinity and ionization potential of the (6,5) s-SWCNT sample. Additionally, at the single-species level, s-SWCNT optical absorption spectra have narrow excitonic resonances (that overlap little with perovskite absorption features) that facilitate the temporal tracking of charge and exciton populations with time-resolved spectroscopy.

Interfacial Band Alignment at the SWCNT−Perovskite Interface. Our first study looked primarily at the detailed band

DOI: 10.1021/acsenergylett.7b00228
ACS Energy Lett. 2017, 2, 1598−1613

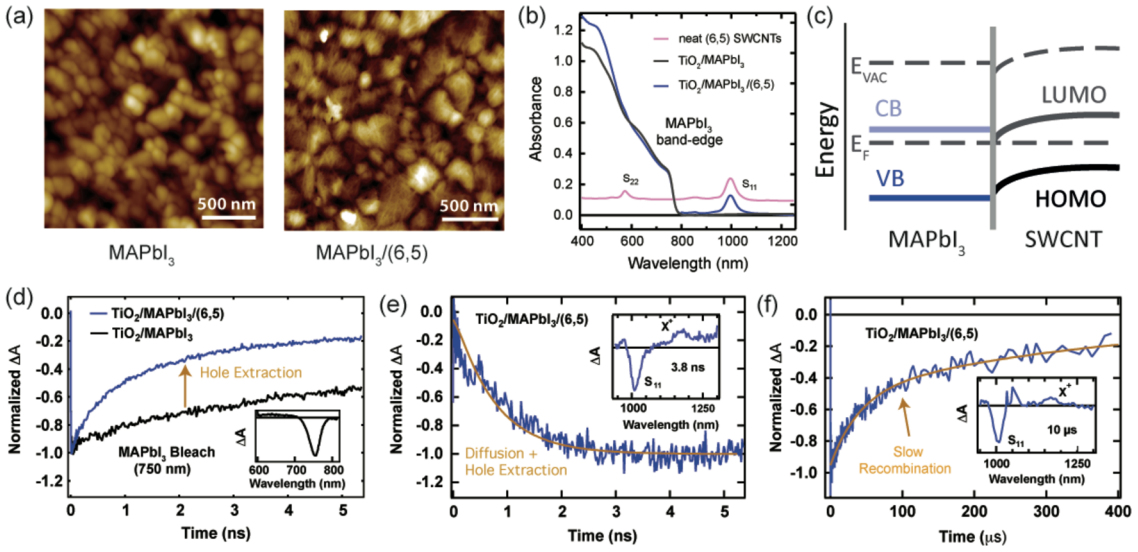

Figure 5. Thermodynamics and excited-state kinetics of the s-SWCNT−perovskite interface. (a) AFM images of the $MaPbI_3$ surface without (left) and with (right) a (6,5) s-SWCNT layer. (b) Absorption spectra of neat (6,5) s-SWCNTs, the neat $MAPbI_3$ film, and the $MAPbI_3$ film with the (6,5) layer. (c) Schematic of interfacial band bending in the (6,5) s-SWCNT layer at the SWCNT−$MAPbI_3$ interface, as measured by photoelectron spectroscopy. (d) Tracking hole extraction at the SWCNT−$MAPbI_3$ interface using the $MAPbI_3$ bleach at 750 nm (inset). (e) Tracking hole extraction at the SWCNT−$MAPbI_3$ interface using the (6,5) S_{11} bleach at 1000 nm (inset). The slow rise of the signal can be modeled to extract the hole diffusion constant and diffusion length within the $MAPbI_3$ layer (gold trace). (f) Tracking hole back transfer and recombination at the SWCNT−$MAPbI_3$ interface (following hole extraction by (6,5) SWCNTs) using the (6,5) SWCNT bleach at 1000 nm (inset). (Figures adapted from ref 93 with permission from the Royal Society of Chemistry).

alignment at the s-SWCNT−perovskite interface, using photoemission spectroscopy.[94] Ultrasonic spraying of the (6,5) s-SWCNT HTM gives us fine nanometer-scale control over the HTM thickness, enabling the deposition of s-SWCNT HTMs with thicknesses varying from 2 to 20 nm (Figure 5a,b). For every s-SWCNT thickness, we utilized (1) ultraviolet photoemission spectroscopy (UPS) to follow the work function and valence band region and (2) X-ray photoemission spectroscopy (XPS) to examine core-level spectra of both the perovskite and SWCNT layers. These measurements uncovered some important properties of the s-SWCNT−$MAPbI_3$ interface. First, the measurements demonstrated that there is no energetic barrier for hole extraction at the s-SWCNT−$MAPbI_3$ interface. Second, the measurements demonstrated that the Fermi energy of (6,5) s-SWCNT layers sprayed onto $MAPbI_3$ systematically changed as the thickness of this layer was increased. The thinnest layers were n-type, but the Fermi energy shifted back to p-type as the thickness increased to 20 nm. Such variation was not observed for (6,5) thin films sprayed on gold reference substrates, in which case they were p-type for all thicknesses, indicating that interactions at the s-SWCNT−perovskite interface induced these variations. Core-level spectra indicated that the most likely explanation for this effect could be traced to a ground-state electron transfer from the methylammonium moiety in the perovskite active layer to the (6,5) s-SWCNTs in the immediate vicinity of the interface. The lead and iodine core levels did not change, indicating that the primary interaction at this interface occurred between the two organic components.

The ultimate result of the interfacial dipole formed at the s-SWCNT−perovskite interface is beneficial band bending within the s-SWCNT layer. In this case, the s-SWCNT valence band levels are shifted toward vacuum as a function of distance from the $MAPbI_3$−s-SWCNT interface (Figure 5c). Importantly, this band bending leads to a ∼0.4 eV barrier for a hole to traverse from the s-SWCNT layer back into the $MAPbI_3$ layer once it is extracted by the s-SWCNT HTM. Thus, the interfacial band alignment uncovered by photoemission measurements suggests that (1) highly enriched s-SWCNT networks (typified by a model (6,5) s-SWCNT system) should be able to extract holes via barrier-free charge transfer from a model perovskite active layer and (2) once extracted, the holes in the s-SWCNT network must surmount a sizable energetic barrier for back transfer into the perovskite active layer.

Photoinduced Interfacial Charge Transfer at the SWCNT−Perovskite Interface. We next utilized time-resolved spectroscopy to study the influence of the interfacial thermodynamics on the kinetics of excited-state charge transfer across the $MAPbI_3$−s-SWCNT interface for a 240 nm thick $MAPbI_3$ active layer (Figure 5d−f).[93] In this case, the spectrally narrow excitonic resonances of the model (6,5) s-SWCNT HTM, in particular, for the S_{11} exciton bleach and the trion induced absorption, served as sensitive indicators of the arrival of holes in the (6,5) HTM following photoexcitation of the perovskite active layer. Additionally, following the temporal evolution of the $MAPbI_3$ exciton bleach at ∼750 nm afforded simultaneous tracking of the charge carrier population within the perovskite active layer (Figure 5d). The perovskite layer was excited at relatively low fluence through the side opposite that where the s-SWCNT HTM was deposited, such that a negligible exciton population was generated in the s-SWCNT layer *and* the bulk of the hole population must diffuse to the interface before being transferred to the (6,5) nanotubes.

Immediate observation of a small signal (both exciton bleach and trion) from the s-SWCNT HTM upon photoexcitation of the $MAPbI_3$ layer demonstrated that the interfacial hole transfer to the s-SWCNT HTM was rapid (subpicosecond), as expected for the barrier-free band alignment discussed above.[94] This small instantaneous signal slowly grew in over the course of several nanoseconds as holes within the $MAPbI_3$ diffused to the s-SWCNT interface and transferred into the (6,5) nanotubes (Figure 5e). Modeling the growth of this signal allowed us to

DOI: 10.1021/acsenergylett.7b00228
ACS Energy Lett. 2017, 2, 1598−1613

estimate a hole diffusion constant of ~0.3 cm^2 s^{-1} and a hole diffusion length of ~1 μm within the $MAPbI_3$ layer. Once extracted, holes were extremely long-lived within the (6,5) HTM, with ~20% of the population still remaining after 400 μs and S_{11} bleach decay time constants of ~40 and 420 μs (Figure 5f). This extremely long-lived charge separation is consistent with the barrier to hole back transfer observed by photoemission measurements (Figure 5c).[94]

Interestingly, we found that the s-SWCNT HTM extracted charges significantly more rapidly than both the spiro-OMeTAD hole extraction layer and the TiO_2 electron extraction layer, as evidenced by control TA measurements at the perovskite band edge (750 nm). For our 240 nm thick perovskite layers, we find that diffusion-limited charge transfer from the photoexcited perovskite layer to either a compact TiO_2 layer or spiro-OMeTAD is relatively inefficient over a 5 ns time scale. These results agree with a number of recent studies that demonstrate poor charge extraction from these "prototypical" charge extraction layers. For example, Leng et al. estimate a hole extraction time constant of ~8 ps for spiro-OMeTAD via TA measurements at 760 nm,[96] whereas our studies demonstrate subpicosecond hole extraction for s-SWCNT HTMs. With regards to electron extraction, several groups have found compact TiO_2 layers to be inefficient in extracting photogenerated electrons from $MAPbI_3$ (especially relative to other layers such as fullerene- and SnO_2-based electron transport materials (ETMs)),[97,98] although they suggest differing mechanisms for the effect. For example, Wojciechowski et al. suggest that electrostatic barriers created by interface states are to blame,[98] whereas Correa Baena et al. suggest that the electron affinity of TiO_2 lies too close to vacuum to extract electrons from $MAPbI_3$, without considering interface states.[97] Finally, our study demonstrated that the extraction of holes by the s-SWCNT HTM actually improved the ability of the compact TiO_2 ETM to subsequently extract electrons from the $MAPbI_3$ active layer.[94] The mechanism for this interesting "cooperative" effect is unclear but is likely related to the beneficial effect that efficient removal of holes by the s-SWCNT HTM has on interfacial kinetics at the TiO_2–$MAPbI_3$ interface and/or the relative energetics of the resulting quasi-Fermi level for electrons in the absence of holes in the active layer.

The fast hole extraction and slow recombination observed for s-SWCNTs on $MAPbI_3$ active layers directly translated to improved device performance.[93] In this case, we used thin (5–15 nm) s-SWCNT interfacial layers between the $MAPbI_3$ active layer and a traditional doped spiro-OMeTAD HTM. The thin interfacial layers significantly improved the device photocurrent, fill factor, and stability and also reduced the hysteresis typically observed between forward and reverse J–V scans (Figure 6). This correlation between interfacial charge transfer kinetics and stability/hysteresis is consistent with a recent study by Ahn et. al that identified interfacial charge trapping as an important mechanism in perovskite device degradation.[99] Considering our own time-resolved measurements and those from the literature,[97−99] minimal J–V hysteresis and improved device stabilities can likely be realized by simultaneously utilizing an ETM and HTM that extract charges rapidly, such as a SnO_2 or fullerene-based ETM paired with SWCNT-based HTM.

Current Prognosis and Future Research Directions. While much progress has been made with regards to using s-SWCNT as absorptive active layers in thin-film solar cells, the efficiencies still remain low (<5% for multispecies and <2% for single-species). This is significantly below the potential efficiencies attainable,

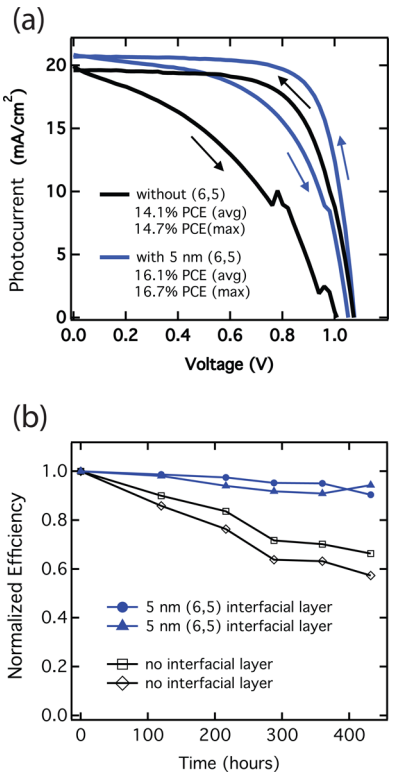

Figure 6. Improvement of perovskite J–V hysteresis and device stability by SWCNTs. A thin (ca. 5 nm) (6,5) s-SWCNT interfacial layer significantly improves the (a) J–V hysteresis and (b) device stability by extracting holes more efficiently than spiro-OMeTAD (Figures adapted from ref 93 with permission from the Royal Society of Chemistry).

given the high absorbance coefficients for s-SWCNTs. As an example, Arnold et al. estimate that a hypothetical 150 nm thick film comprised of 10 s-SWCNT species absorbing at wavelengths shorter than 1200 nm would absorb 86% of the solar spectrum below 1.1 eV (Figure 7a).[28] Tune and Shapter utilized numerical simulations to determine the potential power conversion efficiencies of single-species s-SWCNT PV devices, as well as hypothetical tandem devices fabricated from the combination of four single-species devices.[100] Their simulations, which considered *only* photons harvested by absorption in the s-SWCNTs, revealed that a single-species device with (7,5) s-SWCNTs could attain efficiency in the range of ~7%, whereas a four-species tandem device could attain efficiency as high as 28%.[100] These calculations underscore the potential of solar energy harvesting through the highly absorptive s-SWCNT excitonic transitions.

> The difficulties in bridging the gap between current and potential performance metrics are due, in large part, to many of the unique attributes of s-SWCNTs, especially when fabricated into the macroscopic thin films needed for efficient solar energy harvesting.

The difficulties in bridging the gap between current and potential performance metrics are due, in large part, to many of the unique attributes of s-SWCNTs, especially when fabricated into the

DOI: 10.1021/acsenergylett.7b00228
ACS Energy Lett. 2017, 2, 1598−1613

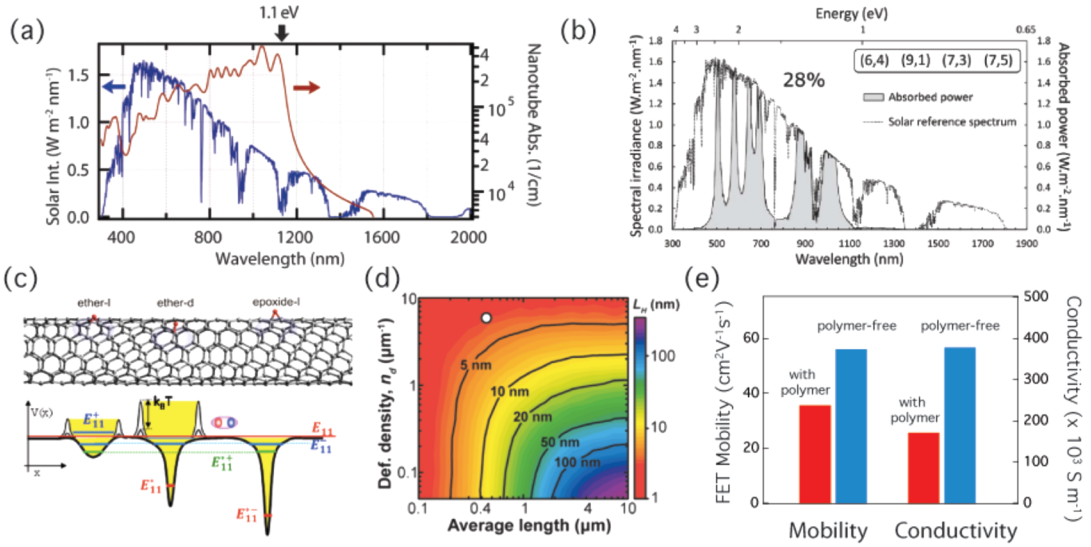

Figure 7. Sunlight harvesting potential of s-SWCNTs and some strategies for approaching this potential in future studies. (a) Modeled absorption spectrum of a polydisperse mixture of 10 s-SWCNTs (red) along with AM1.5 solar spectrum (blue) (Reprinted from ref 28 with permission from the Royal Society of Chemistry). (b) Modeled optical absorption for a tandem solar cell consisting of four individual cells of different (*n*,*m*) species absorbing strongly below 1100 nm. The numerical simulation used in this analysis yields a calculated power conversion efficiency of 28.3% (Reprinted from ref 100 with permission from the Royal Society of Chemistry). (c) (Top) Structure of three different oxygen-related adducts on a segment of (6,5) SWCNT. Schematic of the potential profile along the length of the tube showing potential traps (exciton sinks) created by each of these adducts (Reprinted with permission from ref 104 Copyright 2016 American Chemical Society). (d) Simulated exciton harvesting depth (L_H) as a function of average s-SWCNT length and defect density. The white circle represents an estimate of L_H for a typical (7,5) s-SWCNT thin film, as determined by Wang et al. (Reprinted with permission from ref 107 Copyright 2016 American Chemical Society). (e) FET mobility and maximum electrical conductivity for thin films of s-SWCNTs, where the films contain residual sorting polymer (~50% by mass) or the sorting polymer has been completely removed following film deposition.

macroscopic thin films needed for efficient solar energy harvesting. S-SWCNTs are essentially 100% surface, implying that both environment-related nonradiative exciton recombination rates and interfacial charge carrier recombination rates can be quite high. In deposited thin films, the s-SWCNTs tend to orient predominantly within the plane of the film, the opposite of what is desired for efficient transport of excitons and charges in the cross-plane direction. The high intratube exciton and charge carrier diffusion lengths imply that these quasi-particles sample hundreds of nanometers or more along a nanotube (or bundle) during their lifetime. This can amplify the deleterious effects of exciton and charge carrier trapping, even for extremely small defect densities. Just as many of the positive attributes of s-SWCNTs make them quite promising for solar energy harvesting, these less ideal attributes present the community with a compelling set of fundamental challenges to overcome. Some of the primary challenges are discussed here: improving the length scale over which excitons are harvested, understanding the effects of defects on primary photochemical events such as transport, trapping, and recombination of excitons and charges, and understanding the effects of non-nanotube impurities (e.g., wrapping polymers) and interfacial properties on these same primary photochemical events.

An important reason for the current deficiency in PV device efficiencies for s-SWCNT absorber layers is the short diffusion lengths for excitons in the direction transverse to the plane of a typical s-SWCNT thin film. Whereas the intrananotube exciton diffusion length can be hundreds of nanometers, this value drops precipitously to ~5−10 nm for the internanotube exciton diffusion length within a thin film. One potential solution to this issue is for highly enriched s-SWCNT thin films to be deposited with alignment of the s-SWCNTs perpendicular to the underlying transparent conducting substrate (e.g., FTO). As demonstrated in Figure 7a, these aligned s-SWCNT "forests" would not need to be very tall and could certainly be shorter than the frequently reported range for the s-SWCNT intratube exciton diffusion length (<200 nm) to nearly quantitatively capture the available solar spectrum. Unfortunately, there have been no successful attempts to realize this type of macroscopic vertical alignment for highly pure s-SWCNTs. There are many examples of growing aligned forests of carbon nanotubes, primarily by chemical vapor deposition.[101] Yet, none of these examples have demonstrated specificity for the growth of s-SWCNTs; many of these syntheses result in few-walled or multiwalled CNTs, and the syntheses that result in aligned SWCNT forests contain a statistical ratio of 1/3 m-SWCNTs. Because these m-SWCNTs would short-circuit a PV device, these samples are not useful for thin-film PV devices. There have been reports of postsynthesis methods for selectively removing m-SWCNTs via electrical breakdown,[102] but it is unclear if these strategies could ever be refined to a point where m-SWCNTs were quantitatively removed from forests. It is thus a challenge to the community to come up with creative ways for growing or fabricating highly aligned and highly pure s-SWCNT forests. One could envision some of the necessary steps, such as anchoring separated s-SWCNTs to substrates at tube ends and/or growing forests of s-SWCNTs from small vertically anchored "seeds" with specific electronic structures. Perhaps there are also synthesis

It is thus a challenge to the community to come up with creative ways for growing or fabricating highly aligned and highly pure s-SWCNT forests.

DOI: 10.1021/acsenergylett.7b00228
ACS Energy Lett. 2017, 2, 1598−1613

conditions (e.g., mildly oxidizing) that hinder the growth of m-SWCNTs or selectively etch m-SWCNTs during CVD forest growth.

The effects of defect levels on exciton and charge carrier transport are also still poorly understood in s-SWCNT active layers. Our recent studies suggest that recombination is mediated by trap states,[59] but the identity of these trap states and their effect on exciton/charge transport are still unclear. A number of recent studies have demonstrated that sp^3 sidewall defects on s-SWCNTs generate localized exciton sinks with energies in the range of 150−300 meV below the optically bright singlet exciton level (Figure 7c).[11,103−106] Upon initial submission of this Perspective, no studies had considered the impact these sp^3-related defect sites may have on the exciton harvesting length within electronically coupled s-SWCNT thin films. However, a new study by Wang et al. used diazonium-functionalized polyfluorene-wrapped (7,5) s-SWCNTs as a model system with systematically controlled sp^3 defect density.[107] They showed that moderate levels of covalent sp^3 defects led to a 5-fold reduction of the EQE for s-SWCNT−C_{60} bilayer solar cells.[107] While this study considers diazonium-functionalized s-SWCNTs as a model system, oxygen-related sp^3 defects produce exciton traps with similar depths (Figure 7c).[11,106] Thus, the nearly universal practice of processing SWCNTs in ambient conditions via high-intensity ultrasonic shear implies that at least low levels of oxygen-related defects may be ubiquitous in s-SWCNT dispersions and thin films. The Monte Carlo model developed by Wang et al. suggests that even very low levels of defect densities (at a level of ∼1 sp^3 defect per micron of s-SWCNT) can limit the exciton harvesting length to less than 10 nm for s-SWCNTs with lengths of 1 μm or shorter (Figure 7d).[107] Reducing this defect density to a value of ∼0.1 μm^{-1} while simultaneously maintaining long (>2 μm) s-SWCNTs can dramatically increase the exciton harvesting depth 10- to 20-fold, to ∼100 nm.[107] Looking forward, these considerations suggest that maintaining very mild conditions in the initial debundling and dispersion step, for example, by employing shear force mixing[108] (instead of tip sonication) in rigorously oxygen-free conditions, may significantly boost exciton capture lengths by maintaining long and relatively defect-free s-SWCNTs.

The mechanisms underlying charge separation and recombination in s-SWCNT-based active layers are still at a fledgling level of understanding. As with all organic PV active layers, it is puzzling how truly free charges are generated in such a low-dielectric medium, instead of charges that are separated across the donor−acceptor interface, but still bound by a Coulomb potential. In typical polymer-based OPV active layers, such electron−hole pairs are often described as "bound interfacial radical pairs" or "charge transfer states"[109,110] and in some cases have been identified spectroscopically as low-energy optical transitions with very low oscillator strength. Such entities are still completely unexplored in s-SWCNT active layers and to our knowledge have not been observed spectroscopically. In polymer−fullerene solar cells, it is thought that the maximum open-circuit voltage may be directly related to the energy of the charge transfer state.[109] Thus, detailed study of the energetic landscape at s-SWCNT−acceptor interfaces and the effect of these thermodynamics on carrier recombination is a fruitful direction.

In further probing the energetic landscape of these active layers, it is also important to consider the impact of the sp^3 defects described above, along with dangling bonds at s-SWCNT ends, on carrier transport, trapping, and recombination. While the energy of sp^3 defect-induced exciton levels has now been explored in detail by multiple groups, the energy of single-particle midgap states (i.e., electron and hole trap states) is relatively unexplored, to our knowledge, either experimentally or theoretically. It is important to point out that the open-circuit voltages measured for single-species (e.g., (7,5)) s-SWCNT−C_{60} bilayer solar cells are significantly lower than what should be achievable.[60,68] This deficiency may be related, in part, to trap-mediated recombination,[59] which lowers the quasi-Fermi energy of charge carriers. Thus, it would be very useful to study (1) the carrier density-dependent transport within single-species s-SWCNT films and (2) time-resolved studies on carrier recombination in single-species s-SWCNT−C_{60} bilayers, where the s-SWCNTs in each of these studies are either systematically modified with varying levels of covalent sp^3 defects or dispersed with the mild conditions described above. It is also feasible that unique trap states are created at the interface between s-SWCNTs and acceptors such as fullerenes. As with the charge transfer excitations discussed above, we suggest that the theoretical and experimental exploration of such interface-specific electronic levels represents a fruitful future direction for these PV active layers. These interface states may be particularly important for bulk heterojunction (BHJ) s-SWCNT−fullerene devices. While these devices are a potential solution to the problem of poor exciton harvesting depths, they also have significantly more interfacial contact area, which can exacerbate issues of recombination through interface-related midgap states. It is important to note that, while this BHJ configuration has produced more efficient devices than single-species bilayer devices, the fill factors in BHJ devices are significantly reduced (∼35% in BHJ devices[61] versus ∼60% in bilayer devices[60,66]). In their recent study across 15 different OPV donor−acceptor combinations, Bartesaghi et al. suggest that the competition between recombination and extraction of free charges correlates well with the device fill factor.[111]

Another uncertainty with regards to s-SWCNT active layers is the effect of what can be generally termed the immediate dielectric environment. Broadly speaking, the highly enriched s-SWCNT samples used for energy harvesting thin films can be produced by either aqueous or organic solvent-based separations. Organic-based separations, namely, selective extraction using polyfluorene-based polymers, have produced the most efficient monochiral devices, but it not intuitively clear why this is the case. One potential detriment for aqueous-based separations is the known propensity of water molecules and protons to adsorb on both the s-SWCNT exterior and within the endohedral volume. Such adsorption is known to dope p-type s-SWCNTs and increase nonradiative exciton recombination.[112] In organic polyfluorene-based separations, the polyfluorene polymer is difficult to remove quantitatively; therefore, s-SWCNT networks typically have significant polymer remaining in the thin film, at a mass concentration of up to 50%. Recent studies have demonstrated that this residual polymer can significantly reduce exciton diffusion lengths within s-SWCNT networks[73] and that the particular identity of the polymer may even play a role in transport properties.[74] However, because these studies are sometimes performed by comparing polyfluorene-extracted s-SWCNTs to s-SWCNTs obtained via aqueous separation procedures,[73] it is difficult to draw concrete conclusions regarding the ultimate improvements that may be realized by full removal of the wrapping polymers.

Importantly, several groups have recently demonstrated wrapping polymers with relatively weak intermonomer bonds

DOI: 10.1021/acsenergylett.7b00228
ACS Energy Lett. 2017, 2, 1598−1613

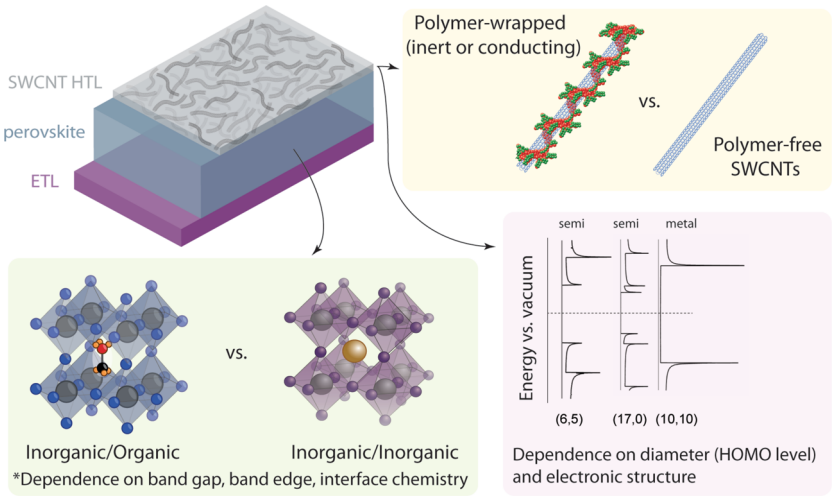

Figure 8. Suggestions of future studies to better understand the thermodynamics and kinetics of model perovskite−SWCNT interfaces, as discussed in detail in the main text.

(e.g., either H-bonds or imines) that can be "decomposed" into monomers by simple treatment with a weak acid such as trifluoroacetic acid (TFA).[50,51,113] Our own recent studies demonstrate dramatic improvements to electrical transport for polydisperse s-SWCNT networks when using such removable polymers, suggesting that residual polyfluorene polymers tend to reduce charge carrier mobility (Figure 7e).[20] We suggest that the next logical step toward improving s-SWCNT PV active layers is the application of these removable polymers to the extraction of the narrow small-diameter s-SWCNT populations that have produced the most efficient PV devices to date. It is also feasible that these studies may elucidate the role of the wrapping polymer in other processes beyond charge/exciton transport, such as the possible role that the polymers may play in either interfacial charge transfer or recombination kinetics.

Many of the purely materials-based questions discussed above for SWCNT active layers are also relevant for SWCNT charge extraction layers in perovskite solar cells. As one example, any processing modification (e.g., using removable wrapping polymers, identifying defect levels) that generally improves charge transport in SWCNT films will likely improve the performance of a SWCNT-based charge extraction layer. However, such modifications may have unintended consequences for an interface that is still poorly understood mechanistically. For example, the role that the wrapping polymer plays in facilitating charge extraction and/or inhibiting recombination is still unclear. To date, most device studies have used SWCNT HTMs where the SWCNTs were dispersed with P3HT,[83,84] whereas our recent time-resolved studies utilize polyfluorene-based polymers.[93,94] P3HT has been demonstrated to be a good single-component hole extraction layer for $MAPbI_3$ devices;[114] therefore, it is unclear if this polymer plays any role in charge extraction and/or recombination when used in concert with SWCNTs in a composite HTM. It is also feasible that wide-gap polyfluorenes in some cases may help to establish an energetic interfacial barrier for recombination. To further clarify the role of wrapping polymers in SWCNT HTMs, future studies are needed that compare the use of both "inert" (e.g., polyfluorenes) and "active" polymers (e.g., P3HT) that remain in the SWCNT film, as well as fully removable polymers (Figure 8).

There are also a number of open questions regarding the mechanistic function and broad applicability of both SWCNT thin films and other HTMs in perovskite solar cells. For example, how universally can SWCNTs be used as HTMs for perovskite-based absorbers? In other words, when we change the identity of the perovskite absorber, what changes are required for the electronic properties of the SWCNT HTM? For example, can SWCNT-based HTMs effectively extract charges from widely varying inorganic/organic active layers where the perovskite band gap increases by >1 V relative to $MAPbI_3$ and/or from inorganic/inorganic perovskite active layers where the interfacial chemistry may deviate substantially from inorganic/organic layers? While it is intuitive to envision that the SWCNT band gap and band edge positions are important for optimizing charge extraction at the perovskite−SWCNT interface, especially when the band gap/band edge positions of the perovskite change appreciably, there are currently no data to support this hypothesis. Some studies have even suggested that large changes in band edge positions for a series of organic HTMs do not appreciably affect device voltage or power conversion efficiency, suggesting Fermi level pinning at the perovskite−HTM interface.[115] S-SWCNT samples with varying diameter and Fermi energy could help probe this effect in greater detail.

Furthermore, our time-resolved studies have focused thus far on purely semiconducting SWCNT HTMs, demonstrating interfacial band bending, fast hole extraction, and very slow recombination. It remains to be seen if these beneficial traits exist for HTMs composed of m-SWCNTs or mixed samples with both types of nanotubes. Intuitively, one might think that m-SWCNTs, which are conducting in their ground state, would produce a HTM with lower series resistance. However, one might also expect that m-SWCNTs could perhaps promote recombination at the SWCNT−perovskite interface. DFT calculations have even predicted for other absorber layers such as CdTe that ground-state charge transfer (such as that observed in our photoelectron spectroscopy experiments) between s-SWCNTs (but not m-SWCNTs) and the semiconductor absorber produces the appropriate energetics for charge extraction.[82] Thus, systematic spectroscopy and device studies are needed that compare SWCNT HTMs with widely varying electronic structure, including (1) varying ratios of m- and s-SWCNTs, (2) varying diameters (and hence band gap/band edges) of s-SWCNTs, and (3) varying perovskite composition and band gap (Figure 8).

DOI: 10.1021/acsenergylett.7b00228
ACS Energy Lett. 2017, 2, 1598−1613

The implications of answering the fundamental questions discussed above for interfaces between perovskite absorber layers and charge extraction layers are quite significant as this system represents a viable pathway toward inexpensive, solution-processed solar cells with efficiencies rivaling or exceeding those of the current silicon devices that dominate the market. SWCNT hole transport layers represent a versatile model system with well-defined electrical and optical properties that can aid in probing the thermodynamic and kinetic factors that foster high efficiency and stability in these promising devices. Organic charge extraction layers have shown tremendous promise for extraction of both charge carrier types and improvement of perovskite device stability, and it is entirely feasible that this application may be one of the first to capitalize on the unique properties of SWCNTs in a widely deployed PV technology.

The implications of answering the fundamental questions discussed here for interfaces between perovskite absorber layers and charge extraction layers are quite significant as this system represents a viable pathway toward inexpensive, solution-processed solar cells with efficiencies rivaling or exceeding those of the current silicon devices that dominate the market.

In summary, the recent progress in separating highly pure single- and few-species samples of semiconducting SWCNTs has enabled detailed fundamental studies on how these novel semiconductors harvest solar energy. In particular, the formation of well-characterized heterojunctions between s-SWCNTs and other organic or inorganic semiconductors affords a careful correlation between the thermodynamic and kinetic aspects of interfaces designed to produce high yields of long-lived separated charges. The understanding gleaned from these studies can inform the rational design of solar energy harvesting systems containing s-SWCNTs and/or other nanoscale semiconductors, toward the ultimate goal of efficient and inexpensive PVs and solar fuels.

AUTHOR INFORMATION

Corresponding Author

*E-mail: jeffrey.blackburn@nrel.gov.

ORCID

Jeffrey L. Blackburn: 0000-0002-9237-5891

Notes

The author declares no competing financial interest.

Biography

Jeff Blackburn is a Senior Scientist and Group Manager of the Spectroscopy and Photoscience Group at the National Renewable Energy Laboratory. His group explores the fundamental properties of a variety of quantum-confined nanomaterials and how these nanomaterials interconvert optical, electrical, and thermal energy.

ACKNOWLEDGMENTS

This Perspective describes work that was funded by the Solar Photochemistry Program, Division of Chemical Sciences, Geosciences, and Biosciences, Office of Basic Energy Sciences, U.S. Department of Energy (DOE). NREL is supported by the DOE under Contract No. DE-AC36- 08GO28308. We are very grateful for the continued support of this work by the Office of Science. The U.S. Government retains (and the publisher, by accepting the article for publication, acknowledges that the U.S. Government retains) a nonexclusive, paid up, irrevocable, worldwide license to publish or reproduce the published form of this work, or allow others to do so, for U.S. Government purposes. The author also acknowledges the many fruitful conversations and collaborations with numerous colleagues that impacted the insights and opinions expressed in this Perspective.

REFERENCES

(1) Iijima, S. Helical Microtubules of Graphitic Carbon. *Nature* **1991**, *354*, 56−58.
(2) Iijima, S.; Ichihashi, T. Single-Shell Carbon Nanotubes of 1-Nm Diameter. *Nature* **1993**, *363*, 603−605.
(3) Arnold, M. S.; Green, A. a.; Hulvat, J. F.; Stupp, S. I.; Hersam, M. C. Sorting Carbon Nanotubes by Electronic Structure Using Density Differentiation. *Nat. Nanotechnol.* **2006**, *1*, 60−65.
(4) Nish, A.; Hwang, J.-Y.; Doig, J.; Nicholas, R. J. Highly Selective Dispersion of Single-Walled Carbon Nanotubes Using Aromatic Polymers. *Nat. Nanotechnol.* **2007**, *2*, 640−646.
(5) Tanaka, T.; Urabe, Y.; Nishide, D.; Kataura, H. Continuous Separation of Metallic and Semiconducting Carbon Nanotubes Using Agarose Gel. *Appl. Phys. Express* **2009**, *2*, 125002.
(6) Tu, X.; Manohar, S.; Jagota, A.; Zheng, M. DNA Sequence Motifs for Structure-Specific Recognition and Separation of Carbon Nanotubes. *Nature* **2009**, *460*, 250−253.
(7) Khripin, C. Y.; Fagan, J. a.; Zheng, M. Spontaneous Partition of Carbon Nanotubes in Polymer-Modified Aqueous Phases. *J. Am. Chem. Soc.* **2013**, *135*, 6822−6825.
(8) Mistry, K. S.; Larsen, B. A.; Blackburn, J. L. High-Yield Dispersions of Large-Diameter Semiconducting Single-Walled Carbon Nanotubes with Tunable Narrow Chirality Distributions. *ACS Nano* **2013**, *7*, 2231−2239.
(9) Diao, S.; Blackburn, J. L.; Hong, G.; Antaris, A. L.; Chang, J.; Wu, J. Z.; Zhang, B.; Cheng, K.; Kuo, C. J.; Dai, H. Fluorescence Imaging in Vivo at Wavelengths Beyond 1500 Nm. *Angew. Chem.* **2015**, *127*, 14971−14975.
(10) Diao, S.; Hong, G.; Antaris, A. L.; Blackburn, J. L.; Cheng, K.; Cheng, Z.; Dai, H. Biological Imaging without Autofluorescence in the Second near-Infrared Region. *Nano Res.* **2015**, *8*, 3027−3034.
(11) Ghosh, S.; Bachilo, S. M.; Simonette, R. A.; Beckingham, K. M.; Weisman, R. B. Oxygen Doping Modifies near-Infrared Band Gaps in Fluorescent Single-Walled Carbon Nanotubes. *Science* **2010**, *330*, 1656−1659.
(12) Sarpkaya, I.; Ahmadi, E. D.; Shepard, G. D.; Mistry, K. S.; Blackburn, J. L.; Strauf, S. Strong Acoustic Phonon Localization in Copolymer-Wrapped Carbon Nanotubes. *ACS Nano* **2015**, *9*, 6383−6393.
(13) Bodiou, L.; Gu, Q.; Guézo, M.; Delcourt, E.; Batté, T.; Lemaitre, J.; Lorrain, N.; Guendouz, M.; Folliot, H.; Charrier, J.; et al. Guided Photoluminescence from Integrated Carbon-Nanotube-Based Optical Waveguides. *Adv. Mater.* **2015**, *27*, 6181−6186.
(14) Pyatkov, F.; Fütterling, V.; Khasminskaya, S.; Flavel, B. S.; Hennrich, F.; Kappes, M. M.; Krupke, R.; Pernice, W. H. P. Cavity-Enhanced Light Emission from Electrically Driven Carbon Nanotubes. *Nat. Photonics* **2016**, *10*, 420−427.
(15) Ma, X.; Hartmann, N. F.; Baldwin, J. K. S.; Doorn, S. K.; Htoon, H. Room-Temperature Single-Photon Generation from Solitary Dopants of Carbon Nanotubes. *Nat. Nanotechnol.* **2015**, *10*, 671−675.
(16) Brady, G. J.; Joo, Y.; Wu, M.-Y.; Shea, M. J.; Gopalan, P.; Arnold, M. S. Polyfluorene-Sorted, Carbon Nanotube Array Field-Effect Transistors with Increased Current Density and High on/Off Ratio. *ACS Nano* **2014**, *8*, 11614−11621.

DOI: 10.1021/acsenergylett.7b00228
ACS Energy Lett. 2017, 2, 1598−1613

(17) Brady, G. J.; Way, A. J.; Safron, N. S.; Evensen, H. T.; Gopalan, P.; Arnold, M. S. Quasi-Ballistic Carbon Nanotube Array Transistors with Current Density Exceeding Si and Gaas. *Sci. Adv.* **2016**, *2*, e1601240.
(18) Franklin, A. D. Nanomaterials in Transistors: From High-Performance to Thin-Film Applications. *Science* **2015**, *349*, aab2750.
(19) Avery, A. D.; Zhou, B. H.; Lee, J.; Lee, E.-S.; Miller, E. M.; Ihly, R.; Wesenberg, D.; Mistry, K. S.; Guillot, S. L.; Zink, B. L.; et al. Tailored Semiconducting Carbon Nanotube Networks with Enhanced Thermoelectric Properties. *Nat. Energy* **2016**, *1*, 16033.
(20) Norton-Baker, B.; Ihly, R.; Gould, I. E.; Avery, A. D.; Owczarczyk, Z. R.; Ferguson, A. J.; Blackburn, J. L. Polymer-Free Carbon Nanotube Thermoelectrics with Improved Charge Carrier Transport and Power Factor. *ACS Energy Lett.* **2016**, *1*, 1212−1220.
(21) Wei, X.; Tanaka, T.; Yomogida, Y.; Sato, N.; Saito, R.; Kataura, H. Experimental Determination of Excitonic Band Structures of Single-Walled Carbon Nanotubes Using Circular Dichroism Spectra. *Nat. Commun.* **2016**, *7*, 12899.
(22) Luer, L.; Hoseinkhani, S.; Polli, D.; Crochet, J.; Hertel, T.; Lanzani, G. Size and Mobility of Excitons in (6, 5) Carbon Nanotubes. *Nat. Phys.* **2009**, *5*, 54−58.
(23) Wang, F.; Dukovic, G.; Brus, L. E.; Heinz, T. F. The Optical Resonances in Carbon Nanotubes Arise from Excitons. *Science* **2005**, *308*, 838−841.
(24) Jorio, A.; Fantini, C.; Pimenta, M. A.; Capaz, R. B.; Samsonidze, G. G.; Dresselhaus, G.; Dresselhaus, M. S.; Jiang, J.; Kobayashi, N.; Grüneis, A.; et al. Resonance Raman Spectroscopy (N,M)-Dependent Effects in Small-Diameter Single-Wall Carbon Nanotubes. *Phys. Rev. B: Condens. Matter Mater. Phys.* **2005**, *71*, 075401.
(25) Dürkop, T.; Getty, S. A.; Cobas, E.; Fuhrer, M. S. Extraordinary Mobility in Semiconducting Carbon Nanotubes. *Nano Lett.* **2004**, *4*, 35−39.
(26) Ihly, R.; Mistry, K. S.; Ferguson, A. J.; Clikeman, T. T.; Larson, B. W.; Reid, O. G.; Boltalina, O. V.; Strauss, S. H.; Rumbles, G.; Blackburn, J. L. Tuning the Driving Force for Exciton Dissociation in Single-Walled Carbon Nanotube Heterojunctions. *Nat. Chem.* **2016**, *8*, 603−609.
(27) Bredas, J. L.; Street, G. B. Polarons, Bipolarons, and Solitons in Conducting Polymers. *Acc. Chem. Res.* **1985**, *18*, 309−315.
(28) Arnold, M. S.; Blackburn, J. L.; Crochet, J. J.; Doorn, S. K.; Duque, J. G.; Mohite, A.; Telg, H. Recent Developments in the Photophysics of Single-Walled Carbon Nanotubes for Their Use as Active and Passive Material Elements in Thin Film Photovoltaics. *Phys. Chem. Chem. Phys.* **2013**, *15*, 14896−14918.
(29) Hofmann, M. S.; Gluckert, J. T.; Noe, J.; Bourjau, C.; Dehmel, R.; Hogele, A. Bright, Long-Lived and Coherent Excitons in Carbon Nanotube Quantum Dots. *Nat. Nanotechnol.* **2013**, *8*, 502−505.
(30) Blackburn, J. L.; Holt, J. M.; Irurzun, V. M.; Resasco, D. E.; Rumbles, G. Confirmation of K-Momentum Dark Exciton Vibronic Sidebands Using 13c-Labeled, Highly Enriched (6,5) Single-Walled Carbon Nanotubes. *Nano Lett.* **2012**, *12*, 1398−1403.
(31) Schöppler, F.; Mann, C.; Hain, T. C.; Neubauer, F. M.; Privitera, G.; Bonaccorso, F.; Chu, D.; Ferrari, A. C.; Hertel, T. Molar Extinction Coefficient of Single-Wall Carbon Nanotubes. *J. Phys. Chem. C* **2011**, *115*, 14682−14686.
(32) Choi, S.; Deslippe, J.; Capaz, R. B.; Louie, S. G. An Explicit Formula for Optical Oscillator Strength of Excitons in Semiconducting Single-Walled Carbon Nanotubes: Family Behavior. *Nano Lett.* **2013**, *13*, 54−58.
(33) Spataru, C. D.; Ismail-Beigi, S.; Capaz, R. B.; Louie, S. G. Theory and Ab Initio Calculation of Radiative Lifetime of Excitons in Semiconducting Carbon Nanotubes. *Phys. Rev. Lett.* **2005**, *95*, 247402.
(34) Capaz, R. B.; Spataru, C. D.; Ismail-Beigi, S.; Louie, S. G. Diameter and Chirality Dependence of Exciton Properties in Carbon Nanotubes. *Phys. Rev. B: Condens. Matter Mater. Phys.* **2006**, *74*, 121401.
(35) Miyauchi, Y.; Oba, M.; Maruyama, S. Cross-Polarized Optical Absorption of Single-Walled Nanotubes by Polarized Photoluminescence Excitation Spectroscopy. *Phys. Rev. B: Condens. Matter Mater. Phys.* **2006**, *74*, 205440.
(36) Matsunaga, R.; Matsuda, K.; Kanemitsu, Y. Origin of Low-Energy Photoluminescence Peaks in Single Carbon Nanotubes: K-Momentum Dark Excitons and Triplet Dark Excitons. *Phys. Rev. B: Condens. Matter Mater. Phys.* **2010**, *81*, 033401.
(37) Torrens, O. N.; Zheng, M.; Kikkawa, J. M. Energy of K-Momentum Dark Excitons in Carbon Nanotubes by Optical Spectroscopy. *Phys. Rev. Lett.* **2008**, *101*, 157401.
(38) Stich, D.; Spath, F.; Kraus, H.; Sperlich, A.; Dyakonov, V.; Hertel, T. Triplet-Triplet Exciton Dynamics in Single-Walled Carbon Nanotubes. *Nat. Photonics* **2013**, *8*, 139−144.
(39) Park, J.; Deria, P.; Olivier, J.-H.; Therien, M. J. Fluence-Dependent Singlet Exciton Dynamics in Length-Sorted Chirality-Enriched Single-Walled Carbon Nanotubes. *Nano Lett.* **2014**, *14*, 504−511.
(40) Dowgiallo, A.-M.; Mistry, K. S.; Johnson, J. C.; Blackburn, J. L. Ultrafast Spectroscopic Signature of Charge Transfer between Single-Walled Carbon Nanotubes and C60. *ACS Nano* **2014**, *8*, 8573−8581.
(41) Dowgiallo, A.-M.; Mistry, K. S.; Johnson, J. C.; Reid, O. G.; Blackburn, J. L. Probing Exciton Diffusion and Dissociation in Single-Walled Carbon Nanotube−C60 Heterojunctions. *J. Phys. Chem. Lett.* **2016**, *7*, 1794−1799.
(42) Ghosh, S.; Bachilo, S. M.; Weisman, R. B. Advanced Sorting of Single-Walled Carbon Nanotubes by Nonlinear Density-Gradient Ultracentrifugation. *Nat. Nanotechnol.* **2010**, *5*, 443−450.
(43) Liu, H.; Nishide, D.; Tanaka, T.; Kataura, H. Large-Scale Single-Chirality Separation of Single-Wall Carbon Nanotubes by Simple Gel Chromatography. *Nat. Commun.* **2011**, *2*, 309.
(44) Fagan, J. A.; Haroz, E. H.; Ihly, R.; Gui, H.; Blackburn, J. L.; Simpson, J. R.; Lam, S.; Hight Walker, A. R.; Doorn, S. K.; Zheng, M. Isolation of >1 Nm Diameter Single-Wall Carbon Nanotube Species Using Aqueous Two-Phase Extraction. *ACS Nano* **2015**, *9*, 5377.
(45) Fagan, J. A.; Huh, J. Y.; Simpson, J. R.; Blackburn, J. L.; Holt, J. M.; Larsen, B. A.; Walker, A. R. H. Separation of Empty and Water-Filled Single-Wall Carbon Nanotubes. *ACS Nano* **2011**, *5*, 3943−3953.
(46) Gui, H.; Streit, J. K.; Fagan, J. A.; Hight Walker, A. R.; Zhou, C.; Zheng, M. Redox Sorting of Carbon Nanotubes. *Nano Lett.* **2015**, *15*, 1642−1646.
(47) Hirano, A.; Tanaka, T.; Urabe, Y.; Kataura, H. Purification of Single-Wall Carbon Nanotubes by Controlling the Adsorbability onto Agarose Gels Using Deoxycholate. *J. Phys. Chem. C* **2012**, *116*, 9816−9823.
(48) Ao, G.; Streit, J. K.; Fagan, J. A.; Zheng, M. Differentiating Left- and Right-Handed Carbon Nanotubes by DNA. *J. Am. Chem. Soc.* **2016**, *138*, 16677−16685.
(49) Shea, M. J.; Mehlenbacher, R. D.; Zanni, M. T.; Arnold, M. S. Experimental Measurement of the Binding Configuration and Coverage of Chirality-Sorting Polyfluorenes on Carbon Nanotubes. *J. Phys. Chem. Lett.* **2014**, *5*, 3742−3749.
(50) Pochorovski, I.; Wang, H.; Feldblyum, J. I.; Zhang, X.; Antaris, A. L.; Bao, Z. H-Bonded Supramolecular Polymer for the Selective Dispersion and Subsequent Release of Large-Diameter Semiconducting Single-Walled Carbon Nanotubes. *J. Am. Chem. Soc.* **2015**, *137*, 4328−4331.
(51) Lei, T.; Chen, X.; Pitner, G.; Wong, H. S. P.; Bao, Z. Removable and Recyclable Conjugated Polymers for Highly Selective and High-Yield Dispersion and Release of Low-Cost Carbon Nanotubes. *J. Am. Chem. Soc.* **2016**, *138*, 802−805.
(52) Toshimitsu, F.; Nakashima, N. Semiconducting Single-Walled Carbon Nanotubes Sorting with a Removable Solubilizer Based on Dynamic Supramolecular Coordination Chemistry. *Nat. Commun.* **2014**, *5*, 5041.
(53) Han, J.; Ji, Q.; Li, H.; Li, G.; Qiu, S.; Li, H.-B.; Zhang, Q.; Jin, H.; Li, Q.; Zhang, J. A Photodegradable Hexaaza-Pentacene Molecule for Selective Dispersion of Large-Diameter Semiconducting Carbon Nanotubes. *Chem. Commun.* **2016**, *52*, 7683−7686.
(54) Toshimitsu, F.; Nakashima, N. Facile Isolation of Adsorbent-Free Long and Highly-Pure Chirality-Selected Semiconducting Single-Walled Carbon Nanotubes Using a Hydrogen-Bonding Supramolecular Polymer. *Sci. Rep.* **2016**, *5*, 18066.
(55) Gregg, B. A. Excitonic Solar Cells. *J. Phys. Chem. B* **2003**, *107*, 4688−4698.

DOI: 10.1021/acsenergylett.7b00228
ACS Energy Lett. 2017, 2, 1598−1613

(56) Ferguson, A. J.; Blackburn, J. L.; Holt, J. M.; Kopidakis, N.; Tenent, R. C.; Barnes, T. M.; Heben, M. J.; Rumbles, G. Photoinduced Energy and Charge Transfer in P3ht:Swnt Composites. *J. Phys. Chem. Lett.* **2010**, *1*, 2406−2411.
(57) Holt, J. M.; Ferguson, A. J.; Kopidakis, N.; Larsen, B. A.; Bult, J.; Rumbles, G.; Blackburn, J. L. Prolonging Charge Separation in P3ht:Swnt Composites Using Highly Enriched Semiconducting Nanotubes. *Nano Lett.* **2010**, *10*, 4627−4633.
(58) Bindl, D. J.; Ferguson, A. J.; Wu, M.-Y.; Kopidakis, N.; Blackburn, J. L.; Arnold, M. S. Free Carrier Generation and Recombination in Polymer-Wrapped Semiconducting Carbon Nanotube Films and Heterojunctions. *J. Phys. Chem. Lett.* **2013**, *4*, 3550−3559.
(59) Ferguson, A. J.; Dowgiallo, A.-M.; Bindl, D. J.; Mistry, K. S.; Reid, O. G.; Kopidakis, N.; Arnold, M. S.; Blackburn, J. L. Trap-Limited Carrier Recombination in Single-Walled Carbon Nanotube Heterojunctions with Fullerene Acceptor Layers. *Phys. Rev. B: Condens. Matter Mater. Phys.* **2015**, *91*, 245311.
(60) Guillot, S. L.; Mistry, K. S.; Avery, A. D.; Richard, J.; Dowgiallo, A.-M.; Ndione, P. F.; van de Lagemaat, J.; Reese, M. O.; Blackburn, J. L. Precision Printing and Optical Modeling of Ultrathin Swcnt/C60 Heterojunction Solar Cells. *Nanoscale* **2015**, *7*, 6556−6566.
(61) Gong, M.; Shastry, T. A.; Xie, Y.; Bernardi, M.; Jasion, D.; Luck, K. A.; Marks, T. J.; Grossman, J. C.; Ren, S.; Hersam, M. C. Polychiral Semiconducting Carbon Nanotube−Fullerene Solar Cells. *Nano Lett.* **2014**, *14*, 5308−5314.
(62) Jain, R. M.; Howden, R.; Tvrdy, K.; Shimizu, S.; Hilmer, A. J.; McNicholas, T. P.; Gleason, K. K.; Strano, M. S. Polymer-Free near-Infrared Photovoltaics with Single Chirality (6,5) Semiconducting Carbon Nanotube Active Layers. *Adv. Mater.* **2012**, *24*, 4436−4439.
(63) Xie, Y.; Gong, M.; Shastry, T. A.; Lohrman, J.; Hersam, M. C.; Ren, S. Broad-Spectral-Response Nanocarbon Bulk-Heterojunction Excitonic Photodetectors. *Adv. Mater.* **2013**, *25*, 3433−3437.
(64) Ramuz, M. P.; Vosgueritchian, M.; Wei, P.; Wang, C.; Gao, Y.; Wu, Y.; Chen, Y.; Bao, Z. Evaluation of Solution-Processable Carbon-Based Electrodes for All-Carbon Solar Cells. *ACS Nano* **2012**, *6*, 10384−10395.
(65) Bindl, D. J.; Wu, M.-Y.; Prehn, F. C.; Arnold, M. S. Efficiently Harvesting Excitons from Electronic Type-Controlled Semiconducting Carbon Nanotube Films. *Nano Lett.* **2011**, *11*, 455−460.
(66) Shea, M. J.; Arnold, M. S. 1% Solar Cells Derived from Ultrathin Carbon Nanotube Photoabsorbing Films. *Appl. Phys. Lett.* **2013**, *102*, 243101.
(67) Ye, Y.; Bindl, D. J.; Jacobberger, R. M.; Wu, M.-Y.; Roy, S. S.; Arnold, M. S. Semiconducting Carbon Nanotube Aerogel Bulk Heterojunction Solar Cells. *Small* **2014**, *10*, 3299−3306.
(68) Bindl, D. J.; Arnold, M. S. Efficient Exciton Relaxation and Charge Generation in Nearly Monochiral (7,5) Carbon Nanotube/C60 Thin-Film Photovoltaics. *J. Phys. Chem. C* **2013**, *117*, 2390−2395.
(69) Pfohl, M.; Glaser, K.; Graf, A.; Mertens, A.; Tune, D. D.; Puerckhauer, T.; Alam, A.; Wei, L.; Chen, Y.; Zaumseil, J. Probing the Diameter Limit of Single Walled Carbon Nanotubes in SWCNT: Fullerene Solar Cells. *Adv. Energy Mater.* **2016**, *6*, 1600890.
(70) Grechko, M.; Ye, Y.; Mehlenbacher, R. D.; McDonough, T. J.; Wu, M.-Y.; Jacobberger, R. M.; Arnold, M. S.; Zanni, M. T. Diffusion-Assisted Photoexcitation Transfer in Coupled Semiconducting Carbon Nanotube Thin Films. *ACS Nano* **2014**, *8*, 5383−5394.
(71) Mehlenbacher, R. D.; McDonough, T. J.; Grechko, M.; Wu, M.-Y.; Arnold, M. S.; Zanni, M. T. Energy Transfer Pathways in Semiconducting Carbon Nanotubes Revealed Using Two-Dimensional White-Light Spectroscopy. *Nat. Commun.* **2015**, *6*, 6732.
(72) Mehlenbacher, R. D.; McDonough, T. J.; Kearns, N. M.; Shea, M. J.; Joo, Y.; Gopalan, P.; Arnold, M. S.; Zanni, M. T. Polarization-Controlled Two-Dimensional White-Light Spectroscopy of Semiconducting Carbon Nanotube Thin Films. *J. Phys. Chem. C* **2016**, *120*, 17069−17080.
(73) Mehlenbacher, R. D.; Wang, J.; Kearns, N. M.; Shea, M. J.; Flach, J. T.; McDonough, T. J.; Wu, M.-Y.; Arnold, M. S.; Zanni, M. T. Ultrafast Exciton Hopping Observed in Bare Semiconducting Carbon Nanotube Thin Films with Two-Dimensional White-Light Spectroscopy. *J. Phys. Chem. Lett.* **2016**, *7*, 2024−2031.
(74) Hartmann, N. F.; Pramanik, R.; Dowgiallo, A.-M.; Ihly, R.; Blackburn, J. L.; Doorn, S. K. Photoluminescence Imaging of Polyfluorene Surface Structures on Semiconducting Carbon Nanotubes: Implications for Thin Film Exciton Transport. *ACS Nano* **2016**, *10*, 11449−11458.
(75) Matsunaga, R.; Matsuda, K.; Kanemitsu, Y. Observation of Charged Excitons in Hole-Doped Carbon Nanotubes Using Photoluminescence and Absorption Spectroscopy. *Phys. Rev. Lett.* **2011**, *106*, 037404.
(76) Park, J. S.; Hirana, Y.; Mouri, S.; Miyauchi, Y.; Nakashima, N.; Matsuda, K. Observation of Negative and Positive Trions in the Electrochemically Carrier-Doped Single-Walled Carbon Nanotubes. *J. Am. Chem. Soc.* **2012**, *134*, 14461−14466.
(77) Kozlov, O. V.; de Haan, F.; Kerner, R. A.; Rand, B. P.; Cheyns, D.; Pshenichnikov, M. S. Real-Time Tracking of Singlet Exciton Diffusion in Organic Semiconductors. *Phys. Rev. Lett.* **2016**, *116*, 057402.
(78) Barnes, T. M.; Bergeson, J. D.; Tenent, R. C.; Larsen, B. A.; Teeter, G.; Jones, K. M.; Blackburn, J. L.; van de Lagemaat, J. Carbon Nanotube Network Electrodes Enabling Efficient Organic Solar Cells without a Hole Transport Layer. *Appl. Phys. Lett.* **2010**, *96*, 243309.
(79) Barnes, T. M.; Reese, M. O.; Bergeson, J. D.; Larsen, B. A.; Blackburn, J. L.; Beard, M. C.; Bult, J.; van de Lagemaat, J. Comparing the Fundamental Physics and Device Performance of Transparent, Conductive Nanostructured Networks with Conventional Transparent Conducting Oxides. *Adv. Energy Mater.* **2012**, *2*, 353−360.
(80) Tenent, R. C.; Barnes, T. M.; Bergeson, J. D.; Ferguson, A. J.; To, B.; Gedvilas, L. M.; Heben, M. J.; Blackburn, J. L. Ultrasmooth, Large-Area, High-Uniformity, Conductive Transparent Single-Walled-Carbon-Nanotube Films for Photovoltaics Produced by Ultrasonic Spraying. *Adv. Mater.* **2009**, *21*, 3210−3216.
(81) van de Lagemaat, J.; Barnes, T. M.; Rumbles, G.; Shaheen, S. E.; Coutts, T. J.; Weeks, C.; Levitsky, I.; Peltola, J.; Glatkowski, P. Organic Solar Cells with Carbon Nanotubes Replacing In2O3:Sn as the Transparent Electrode. *Appl. Phys. Lett.* **2006**, *88*, 233503.
(82) Phillips, A. B.; Khanal, R. R.; Song, Z.; Zartman, R. M.; DeWitt, J. L.; Stone, J. M.; Roland, P. J.; Plotnikov, V. V.; Carter, C. W.; Stayancho, J. M.; et al. Wiring-up Carbon Single Wall Nanotubes to Polycrystalline Inorganic Semiconductor Thin Films: Low-Barrier, Copper-Free Back Contact to Cdte Solar Cells. *Nano Lett.* **2013**, *13*, 5224−5232.
(83) Habisreutinger, S. N.; Leijtens, T.; Eperon, G. E.; Stranks, S. D.; Nicholas, R. J.; Snaith, H. J. Carbon Nanotube/Polymer Composites as a Highly Stable Hole Collection Layer in Perovskite Solar Cells. *Nano Lett.* **2014**, *14*, 5561−5568.
(84) Habisreutinger, S. N.; Leijtens, T.; Eperon, G. E.; Stranks, S. D.; Nicholas, R. J.; Snaith, H. J. Enhanced Hole Extraction in Perovskite Solar Cells through Carbon Nanotubes. *J. Phys. Chem. Lett.* **2014**, *5*, 4207−4212.
(85) Rowell, M. W.; Topinka, M. A.; McGehee, M. D.; Prall, H.-J.; Dennler, G.; Sariciftci, N. S.; Hu, L.; Gruner, G. Organic Solar Cells with Carbon Nanotube Network Electrodes. *Appl. Phys. Lett.* **2006**, *88*, 233506.
(86) Pasquier, A. D.; Unalan, H. E.; Kanwal, A.; Miller, S.; Chhowalla, M. Conducting and Transparent Single-Wall Carbon Nanotube Electrodes for Polymer-Fullerene Solar Cells. *Appl. Phys. Lett.* **2005**, *87*, 203511.
(87) Barnes, T. M.; Wu, X.; Zhou, J.; Duda, A.; van de Lagemaat, J.; Coutts, T. J.; Weeks, C. L.; Britz, D. A.; Glatkowski, P. Single-Wall Carbon Nanotube Networks as a Transparent Back Contact in CdTe Solar Cells. *Appl. Phys. Lett.* **2007**, *90*, 243503.
(88) Contreras, M. A.; Barnes, T.; van de Lagemaat, J.; Rumbles, G.; Coutts, T. J.; Weeks, C.; Glatkowski, P.; Levitsky, I.; Peltola, J.; Britz, D. A. Replacement of Transparent Conductive Oxides by Single-Wall Carbon Nanotubes in Cu(in,Ga)Se2-Based Solar Cells. *J. Phys. Chem. C* **2007**, *111*, 14045−14048.
(89) Jung, Y.; Li, X.; Rajan, N. K.; Taylor, A. D.; Reed, M. A. Record High Efficiency Single-Walled Carbon Nanotube/Silicon P−N Junction Solar Cells. *Nano Lett.* **2013**, *13*, 95−99.

DOI: 10.1021/acsenergylett.7b00228
ACS Energy Lett. 2017, 2, 1598−1613

(90) Tune, D. D.; Hennrich, F.; Dehm, S.; Klein, M. F. G.; Glaser, K.; Colsmann, A.; Shapter, J. G.; Lemmer, U.; Kappes, M. M.; Krupke, R.; et al. The Role of Nanotubes in Carbon Nanotube−Silicon Solar Cells. *Adv. Energy Mater.* **2013**, *3*, 1091−1097.
(91) Tune, D. D.; Flavel, B. S.; Krupke, R.; Shapter, J. G. Carbon Nanotube-Silicon Solar Cells. *Adv. Energy Mater.* **2012**, *2*, 1043−1055.
(92) Li, Z.; Kulkarni, S. A.; Boix, P. P.; Shi, E.; Cao, A.; Fu, K.; Batabyal, S. K.; Zhang, J.; Xiong, Q.; Wong, L. H.; et al. Laminated Carbon Nanotube Networks for Metal Electrode-Free Efficient Perovskite Solar Cells. *ACS Nano* **2014**, *8*, 6797−6804.
(93) Ihly, R.; Dowgiallo, A.-M.; Yang, M.; Schulz, P.; Stanton, N. J.; Reid, O. G.; Ferguson, A. J.; Zhu, K.; Berry, J. J.; Blackburn, J. L. Efficient Charge Extraction and Slow Recombination in Organic-Inorganic Perovskites Capped with Semiconducting Single-Walled Carbon Nanotubes. *Energy Environ. Sci.* **2016**, *9*, 1439−1449.
(94) Schulz, P.; Dowgiallo, A.-M.; Yang, M.; Zhu, K.; Blackburn, J. L.; Berry, J. J. Charge Transfer Dynamics between Carbon Nanotubes and Hybrid Organic Metal Halide Perovskite Films. *J. Phys. Chem. Lett.* **2016**, *7*, 418−425.
(95) Park, N.-G.; Grätzel, M.; Miyasaka, T.; Zhu, K.; Emery, K. Towards Stable and Commercially Available Perovskite Solar Cells. *Nat. Energy* **2016**, *1*, 16152.
(96) Leng, J.; Liu, J.; Zhang, J.; Jin, S. Decoupling Interfacial Charge Transfer from Bulk Diffusion Unravels Its Intrinsic Role for Efficient Charge Extraction in Perovskite Solar Cells. *J. Phys. Chem. Lett.* **2016**, *7*, 5056−5061.
(97) Correa Baena, J. P.; Steier, L.; Tress, W.; Saliba, M.; Neutzner, S.; Matsui, T.; Giordano, F.; Jacobsson, T. J.; Srimath Kandada, A. R.; Zakeeruddin, S. M.; et al. Highly Efficient Planar Perovskite Solar Cells through Band Alignment Engineering. *Energy Environ. Sci.* **2015**, *8*, 2928−2934.
(98) Wojciechowski, K.; Stranks, S. D.; Abate, A.; Sadoughi, G.; Sadhanala, A.; Kopidakis, N.; Rumbles, G.; Li, C.-Z.; Friend, R. H.; Jen, A. K. Y.; et al. Heterojunction Modification for Highly Efficient Organic-Inorganic Perovskite Solar Cells. *ACS Nano* **2014**, *8*, 12701−12709.
(99) Ahn, N.; Kwak, K.; Jang, M. S.; Yoon, H.; Lee, B. Y.; Lee, J.-K.; Pikhitsa, P. V.; Byun, J.; Choi, M. Trapped Charge-Driven Degradation of Perovskite Solar Cells. *Nat. Commun.* **2016**, *7*, 13422.
(100) Tune, D. D.; Shapter, J. G. The Potential Sunlight Harvesting Efficiency of Carbon Nanotube Solar Cells. *Energy Environ. Sci.* **2013**, *6*, 2572−2577.
(101) Robertson, J.; Zhong, G.; Esconjauregui, S.; Zhang, C.; Fouquet, M.; Hofmann, S. Chemical Vapor Deposition of Carbon Nanotube Forests. *Phys. Status Solidi B* **2012**, *249*, 2315−2322.
(102) Collins, P. G.; Arnold, M. S.; Avouris, P. Engineering Carbon Nanotubes and Nanotube Circuits Using Electrical Breakdown. *Science* **2001**, *292*, 706−709.
(103) Piao, Y.; Meany, B.; Powell, L. R.; Valley, N.; Kwon, H.; Schatz, G. C.; Wang, Y. Brightening of Carbon Nanotube Photoluminescence through the Incorporation of Sp3 Defects. *Nat. Chem.* **2013**, *5*, 840−845.
(104) Hartmann, N. F.; Velizhanin, K. A.; Haroz, E. H.; Kim, M.; Ma, X.; Wang, Y.; Htoon, H.; Doorn, S. K. Photoluminescence Dynamics of Aryl Sp3 Defect States in Single-Walled Carbon Nanotubes. *ACS Nano* **2016**, *10*, 8355−8365.
(105) Kim, M.; Adamska, L.; Hartmann, N. F.; Kwon, H.; Liu, J.; Velizhanin, K. A.; Piao, Y.; Powell, L. R.; Meany, B.; Doorn, S. K.; et al. Fluorescent Carbon Nanotube Defects Manifest Substantial Vibrational Reorganization. *J. Phys. Chem. C* **2016**, *120*, 11268−11276.
(106) Ma, X.; Adamska, L.; Yamaguchi, H.; Yalcin, S. E.; Tretiak, S.; Doorn, S. K.; Htoon, H. Electronic Structure and Chemical Nature of Oxygen Dopant States in Carbon Nanotubes. *ACS Nano* **2014**, *8*, 10782−10789.
(107) Wang, J.; Shea, M. J.; Flach, J. T.; McDonough, T. J.; Way, A. J.; Zanni, M. T.; Arnold, M. S. Role of Defects as Exciton Quenching Sites in Carbon Nanotube Photovoltaics. *J. Phys. Chem. C* **2017**, *121*, 8310−8318.
(108) Graf, A.; Zakharko, Y.; Schießl, S. P.; Backes, C.; Pfohl, M.; Flavel, B. S.; Zaumseil, J. Large Scale, Selective Dispersion of Long Single-Walled Carbon Nanotubes with High Photoluminescence Quantum Yield by Shear Force Mixing. *Carbon* **2016**, *105*, 593−599.
(109) Deibel, C.; Strobel, T.; Dyakonov, V. Role of the Charge Transfer State in Organic Donor−Acceptor Solar Cells. *Adv. Mater.* **2010**, *22*, 4097−4111.
(110) Vandewal, K.; Albrecht, S.; Hoke, E. T.; Graham, K. R.; Widmer, J.; Douglas, J. D.; Schubert, M.; Mateker, W. R.; Bloking, J. T.; Burkhard, G. F.; et al. Efficient Charge Generation by Relaxed Charge-Transfer States at Organic Interfaces. *Nat. Mater.* **2013**, *13*, 63−68.
(111) Bartesaghi, D.; Pérez, I. d. C.; Kniepert, J.; Roland, S.; Turbiez, M.; Neher, D.; Koster, L. J. A. Competition between Recombination and Extraction of Free Charges Determines the Fill Factor of Organic Solar Cells. *Nat. Commun.* **2015**, *6*, 7083.
(112) Lee, A. J.; Wang, X.; Carlson, L. J.; Smyder, J. A.; Loesch, B.; Tu, X.; Zheng, M.; Krauss, T. D. Bright Fluorescence from Individual Single-Walled Carbon Nanotubes. *Nano Lett.* **2011**, *11*, 1636−1640.
(113) Lei, T.; Pochorovski, I.; Bao, Z. Separation of Semiconducting Carbon Nanotubes for Flexible and Stretchable Electronics Using Polymer Removable Method. *Acc. Chem. Res.* **2017**, *50*, 1096−1104.
(114) Heo, J. H.; Im, S. H.; Noh, J. H.; Mandal, T. N.; Lim, C.-S.; Chang, J. A.; Lee, Y. H.; Kim, H.-j.; Sarkar, A.; NazeeruddinMd, K.; et al. Efficient Inorganic-Organic Hybrid Heterojunction Solar Cells Containing Perovskite Compound and Polymeric Hole Conductors. *Nat. Photonics* **2013**, *7*, 486−491.
(115) Belisle, R. A.; Jain, P.; Prasanna, R.; Leijtens, T.; McGehee, M. D. Minimal Effect of the Hole-Transport Material Ionization Potential on the Open-Circuit Voltage of Perovskite Solar Cells. *ACS Energy Lett.* **2016**, *1*, 556−560.

DOI: 10.1021/acsenergylett.7b00228
ACS Energy Lett. 2017, 2, 1598−1613